Proposal for an Experiment at PSI (following R-89.01.0)

A PRECISE MEASUREMENT OF THE $\pi^+ \to \pi^0 e^+ \nu$ DECAY RATE

D. Počanić, K.A. Assamagan, J.P. Chen, D. Day, E. Frlež, K.J. Keeter, R.M. Marshall, J.S. McCarthy, J.H. Mitchell, R.C. Minehart, B.E. Norum, O.A. Rondon-Aramayo, L.C. Smith, W.A. Stephens, B.K. Wright, K.O.H. Ziock
University of Virginia, Charlottesville, Virginia 22901, U.S.A.

M. Daum, R. Frosch, D. Renker
PSI, Paul-Scherrer-Institut, CH-5234 Villigen, Switzerland

T. Kozlowski
Institute for Nuclear Studies, PL-05-400 Swierk, Poland

B.G. Ritchie
Arizona State University, Tempe, AZ 85287-1504, U.S.A.

S.M. Korenchenko, N.A. Kuchinsky, N.P. Kravchuk, I.V. Kisel, A.S. Korenchenko, K.G. Nekrasov, D.B. Kozaikin, V.A. Baranov, A. Moiseenko, S. Jakovlev
Joint Institute for Nuclear Research, Dubna, Russia

Yu. Bagaturia, W. Djordjadze, D. Mzavia, G. Melitauri, T. Sachelashvili
Institute for High Energy Physics, Tbilisi State University, Georgia

A. Marušić, T. Petković, I. Supek, I. Šlaus
R. Bošković Institute and University of Zagreb, Zagreb, Croatia

Ch. Broennimann, H. Pruys, R. Engfer
Institut für Physik, Universität Zürich, Switzerland

submitted 27 May 1991, revised 11 Dec. 1991, Dec. 1992

We are proposing an experimental program with the aim of making a precise determination of the pion beta decay rate. The proposed experimental method was designed to achieve an overall level of uncertainty in the range of 0.2 – 0.3%. Due to the complex nature of the proposed measurement, the final objective would be reached in stages. The objective of the first stage will be to improve the accuracy of the pion beta decay rate from the present $\sim$4% to $\sim$0.5%.

Due to the relative simplicity of the studied decay and its radiative corrections, precise knowledge of the pion beta decay rate provides a stringent test of the quark-lepton charged-current universality (through the CVC hypothesis), and the unitarity of the Cabibbo-Kobayashi-Masakawa quark mixing matrix. The latter can be used to constrain certain extensions to the current minimal Standard Model.

The detector system designed for the $\pi\beta$ experiment will also be suitable for improved measurements of the $\pi \to e\nu\gamma$ and $\mu \to e\nu\overline{\nu}\gamma$ decays.

BEAM REQUIREMENTS EXPERIMENTAL AREA: πE1 / πM3

We require a stopped pion beam with the highest stopping density consistent with small spot size, and with the minimal muon and positron contamination. The required pion rates are relatively modest: $< 10^7\pi/\mathrm{s}$. After the PSI accelerator upgrade is fully implemented, it should be possible to satisfy these requirements in at least two beam lines, i.e., πE1 and πM3. The presence of the electrostatic separator in the latter beam line may favor its choice, since the use of πE1 would imply either moving the existing separator from πM3, or acquiring a second separator.

The standard primary beam mode at PSI (micropulses separated by 20 ns) is suitable for the proposed measurements.

Particles: π^+

Momentum: ~100 MeV/c, will be tuned so as to optimize π - μ timing separation

Momentum band: ~1%, subject to requirements outlined above

Size of beam spot: ~1 cm diameter

Intensity: $10^5 - 5 \times 10^6\ \pi/s$

Beam purity: minimal μ^+ and e^+ contamination, < 10%

DURATION OF EXPERIMENT

Due to the low $\pi\beta$ decay branching ratio, the "production running" will require $\sim 2 \times 10^7$ s of beam (or approximately one calendar year taking into account beam off periods). However, before production runs can begin, considerable effort is required in order to build, assemble and calibrate the detectors, as well as to understand and achieve the desired systematic uncertainties and detector performance. The proposed measurements will therefore require a program stretching over several years. However, the work will be done in stages, and the present collaboration is expected to grow over time commensurate to the effort.

At present we are asking for BV approval of the experiment so that we can proceed to obtain equipment funding necessary for building detectors. We will also request beam time for a short development run (3 weeks) in the winter 1991/92 period. The exact scheduling of this beam time will depend on the state of readiness of the prototype CsI calorimeter modules.

SAFETY CONSIDERATIONS

There are no unusual safety risks involved in the proposed measurements.

1. SCIENTIFIC MOTIVATION

1.1. Theoretical predictions and interpretation

Pion beta decay ($\pi^+ \to \pi^0 e^+ \nu$) is one of the fundamental semileptonic weak interaction processes. It is a transition between two spin-zero members of an isospin triplet, and is therefore analogous to superallowed pure Fermi transitions in nuclear beta decay. Due to its relative simplicity and, consequently, accuracy of theoretical description, Fermi beta decay stands today among the prominent successes of the Standard Model of electroweak interactions.

At the tree level, the rate of pure Fermi nuclear beta decay is directly related to the vector coupling constant G_V^2 and the nuclear Fermi matrix element M_F. The conserved vector current hypothesis (CVC) predicts that the product ft of the Fermi integral function f and decay half-life $t_{1/2}$ is a universal constant proportional to G_V^2.

Two types of nucleus-dependent corrections are needed in order to extract G_V from measured decay rates: (a) phase space dependent radiative corrections δ_R due to electroweak and QCD loop diagrams, and (b) nuclear structure dependent corrections δ_C to the matrix element M_F.

In the course of the past two decades radiative corrections of $O(\alpha)$ have been calculated, as well as the leading terms of $O(Z\alpha^2)$, while contributions of $O(Z^2\alpha^3)$ have been estimated [Sir-87a]. The resulting δ_R's amount to ~3-4%, typically, with a theoretical uncertainty of 0.2% arising mainly from short-distance axial-vector-induced contributions [Mar-86].

On the other hand, the nuclear corrections δ_C are smaller, ranging in magnitude from 0.2 to 1%, but their evaluation appears to be accompanied by significant ambiguities [Orm-89]. There have been three systematic evaluations of δ_C, by Towner, Hardy and Harvey [Tow-77], Wilkinson [Wil-78], and Ormand and Brown [Orm-85,89], (which we will label THH, W and OB, respectively). The most recent and theoretically refined is the OB calculation which yields a corrected value of "$\mathcal{F}t$" which is 0.2% (or 3σ) higher than that determined using THH δ_C's. The THH and W results agree within the quoted uncertainties. (We note in passing that the interpretation of $0^+ \to 0^+$ nuclear beta decay results may be further complicated by the recent discovery by Drukarev and Strikman [Dru-87] that β electron final-state interaction effects, primarily Coulomb screening corrections, are more pronounced than previously thought. This effect was found to worsen the agreement between low- and high-Z nuclei, and to move the central value of V_{ud} downward, i.e., away from CKM unitarity.)

The THH-OB discrepancy has intriguing consequences on the unitarity of the Cabibbo-Kobayashi-Masakawa (CKM) quark mixing matrix. Cabibbo universality relates G_V to the muon weak coupling constant G_μ via the CKM matrix element V_{ud}. Using the accepted value for V_{us} [Don-87] and the limit on V_{ub} [Tho-88], as well as the THH δ_C, results in a value of $|V_1|^2 = |V_{ud}|^2 + |V_{us}|^2 + |V_{ub}|^2$ consistent with unity, while the OB δ_C fall short of unity by $\sim 2\sigma$. The discrepancy was removed by Hardy *et al.* [Har-90] who studied the spread of the THH and OB δ_C's, and took unweighted averages, reducing the overall uncertainties accordingly. Using the results of Hardy *et al.* , one obtains $|V_{ud}|^2 + |V_{us}|^2 + |V_{ub}|^2 = 0.9962 \pm 0.0016$, i.e., a value 2.4σ lower than the SM prediction.

V_{ud} can also be determined from neutron beta decay using the τ_n and G_A/G_V. The new precision measurement of the electron asymmetry in neutron decay by Erozolimskiĭ *et al.* [Ero-90] results in the new average for the ratio $G_A/G_V = -1.2570 \pm 0.0028$. Combining this result with the average of the neutron lifetime measurements, 888.8 $\pm$ 2.4 s, one gets $V_{ud} = 0.9804 \pm 0.0022$. The latter value brings $|V_{ud}|^2 + |V_{us}|^2 + |V_{ub}|^2$ up to 1.0096 ± 0.0044, which also differs from the SM prediction by 2.2σ, but in the *opposite* direction.

Thus, the determination of V_{ud} and the test of universality is presently not in a satisfactory state at the level of several tenths of a percent.

Determination of the $\pi^+ \to \pi^0 e^+ \nu$ rate at the level of a few tenths of a percent is, therefore, of clear importance. Already at $\sim$0.5%, such a measurement would provide an important independent test of universality in a meson. It is of particular interest to find out where the pion beta decay result will fall, whether it will be consistent with the nuclear Fermi decays, or with the neutron decay data. There is also a theoretical advantage to the pion beta decay which provides a strong further motivation for a very precise measurement.

Following Källén's CVC calculations for the uncorrected $\pi\beta$ decay rate [Käl-64], Sirlin included the effect of radiative corrections in a current algebra formulation [Sir-78]. For the $\pi\beta$ decay rate he obtained [Sir-78]:

$$\frac{1}{\tau_{\pi\beta}} = \frac{\ln 2}{30(\mathcal{F}t)} \Big[\frac{\Delta}{m_e}\Big]^5 \Big[1 - \frac{\Delta}{2m_+}\Big]^3 f(\epsilon, \Delta)(1 + \delta_\pi^0), \tag{1.1}$$

where:

$$f(\epsilon, \Delta) = \sqrt{1-\epsilon}\,\Big(1 - \frac{9\epsilon}{2} - 4\epsilon^2\Big) + \frac{15}{2}\epsilon^2 \ln\Big(\frac{1+\sqrt{1-\epsilon}}{\sqrt{\epsilon}}\Big)^2 - \frac{3}{7}\Big(\frac{\Delta}{m_+ + m_0}\Big)^2, \tag{1.2}$$

and:

$$\epsilon = \Big(\frac{m_e}{\Delta}\Big)^2 = \Big(\frac{m_e}{m_+ - m_0}\Big)^2. \tag{1.3}$$

The radiative and other corrections discussed for nuclear decays enter into the universal $\mathcal{F}t$ value and the "outer correction" δ_π^0. However, in contrast to nuclear Fermi decays, pion beta decay is altogether free of the nuclear overlap correction δ_C, as well as of the screening correction, and involves a simpler axial-vector contribution to the radiative correction δ_R [Mar-86]. The overall theoretical uncertainty involved in evaluating G_V^2 or $|V_{ud}|^2$ from an experimental pion beta decay rate $\tau_{\pi\beta}^{-1}$ is thus $\leq 0.1\%$ [Mar-86, Sir-89]. The only other significant source of uncertainty in such an evaluation involves the pion mass difference $\Delta = m_{\pi^+} - m_{\pi^0}$. Δ has been recently determined [Cra-88] to an accuracy of 10^{-4}, and thus contributes 0.05% towards a total theoretical uncertainty in $\tau_{\pi\beta}^{-1}$ of $\leq 0.11\%$. This theoretical advantage is, however, offset by considerable experimental difficulties due to the small $\pi\beta$ branching ratio which is of $O(10^{-8})$; hence the experimental accuracy of $\tau_{\pi\beta}^{-1}$ presently stands at 4% [McF-85].

We note parenthetically that a third approach to determining V_{ud} , at present technically least feasible, would involve a precise measurement of the hitherto unobserved rare decay $K_L^0 \to K^\pm e^\mp \overline{\nu}$ [Hig-83]. The expected branching ratio for this decay is also of $O(10^{-8})$. Such an experiment does not appear feasible with the neutral K beams available now.

1.2. Theoretical implications

In order to fully assess the potential value of a precise determination of the $\pi\beta$ decay rate, it is useful to examine the information extracted from the presently available $0^+ \to 0^+$

nuclear beta decay results. These data are already sufficiently precise to verify the validity of the CVC predictions in nuclei at the level of quantum corrections, and to place constraints on certain phenomena outside the present three-generation SM, as follows.

(a) One can look for a signal of a fourth fermion generation through the $V_{ub'}$ mixing inferred from an experimental violation of three-generation CKM unitarity [Mar-86]. CKM unitarity has been discussed above; due to the ambiguities in the nuclear corrections, at present one is led to extract from the data only an upper bound of $V_{ub'} \leq 0.07$ at the 90% confidence limit. However, if one adopts the OB analysis results [Orm-89], a more restrictive limit is obtained: $0.01 \leq V_{ub'} \leq 0.08$ at 90% CL. This matter clearly needs further experimental clarification.

(b) Another possible mechanism for quark-lepton universality violation involves supersymmetric particles. Supersymmetric partners to known particles occur in supersymmetric extensions to the minimal SM. An SM extension along these lines would have considerable aesthetic and theoretical appeal; indeed, several SUSY models have been proposed. However, experimental searches for superparticles in e^+e^- and $p\overline{p}$ collisions have so far produced negative results. Recently Barbieri *et al.* pointed out that superparticle exchanges in μ and β decay give rise to a violation of quark-lepton universality, unless their masses are suitably constrained [Bar-85]. A more careful analysis [Bar-86] by the same authors has shown that significant regions in the ($m_{\tilde{q}}$, $m_{\tilde{\ell}}$, $m_{\widetilde{W}}$) space can be excluded on the basis of presently available superallowed Fermi nuclear β decay data. The sign of the supersymmetric correction δ_S is in the right direction, i.e., it would reduce $|V_{ud}|_{SM}$. For example, given reasonable assumptions on the higgsino mass parameter range, i.e., $m_{\tilde{h}} \geq O(100\text{ GeV})$, the combination $m_{\tilde{q}} = 80$ GeV, $m_{\tilde{\ell}} = 25$ GeV, $m_{\widetilde{W}} = 30$ GeV is excluded.

(c) The existence of additional neutral gauge bosons Z' besides the known γ and Z of the standard $SU(2)_L \otimes U(1)_Y$ electroweak theory would have significant implications for the SM and grand unified theories (GUT's). Marciano and Sirlin have recently computed quantum loop corrections to the quark mixing angles resulting from several types of Z' [Mar-87]. Lower bounds on $m_{Z'}$ ranging from 254 to 413 GeV are obtained, depending on the choice of the GU model for the Z' [Mar-87, Sir-89].

(d) Compositeness of elementary particles, particularly of the fermions and vector gauge bosons which participate in the weak interactions, has been long considered a possible way to extend the SM. Sirlin has recently examined the consequences of several models of compositeness on electroweak radiative loop corrections [Sir-87b]. In this framework, experimental limits on the validity of quark-lepton universality can be used to constrain the mass scale of compositeness to the range above $\Lambda \geq 7$ TeV [Sir-89].

It is important to note that the constraints discussed above are comparably restrictive to those extracted so far from direct high-energy measurements of electroweak processes. Hence, the present level of theoretical accuracy in the interpretation of hadronic β decay processes in principle enables a selective exploration of certain phenomena on a mass scale largely inaccessible to existing (pre-SSC) accelerators [Mar-87, Sir-87b,-89]. A number of authors have therefore recently called for new, more precise measurements of the pion and neutron beta decays in order to push higher the above limits on new physics (cf. e.g., references Sir-87, Mar-86, Bar-85, Mar-87, Sir-87b and Sir-86).

We propose to pursue the goal of improved experimental accuracy in the $\pi\beta$ decay rate, in a staged approach. We believe that the present fundamental relevance of the results of such measurements justifies the significant effort necessary to carry them out. Furthermore, the availability of high-quality intense low-energy pion beams at existing meson facilities (which, however, will not remain in operation indefinitely), as well as recent advances in detector technology, make these measurements timely and feasible at a cost lower than is characteristic of similarly sensitive tests of the SM at higher energies.

1.3. **Previous measurements**

As previously noted, the most recent and most precise determination of the $\pi\beta$ decay rate is due to McFarlane *et al.* [McF-85], who performed an in-flight decay measurement. Their result is:

$$\frac{1}{\tau_{\pi\beta}} = 0.394 \pm 0.015\mathrm{s}^{-1}. \tag{1.5}$$

This result is in good agreement with theoretical predictions, but with a $\sim$4% uncertainty it is insufficiently precise for testing even the full extent of the radiative corrections which stand at $\sim$3% [Sir-78].

The purpose of the present proposal is twofold. First, we intend to bring the experimental uncertainties down to a level $\sim$0.5%, which is well within the level of calculated radiative corrections. This would provide a direct test of the calculations in the simple pion system. At the same time we shall work on minimizing systematic uncertainties in order to make possible a very precise measurement, in the region of $\sim$0.2 – 0.3 % which would provide a stringent test of the CVC and Standard Model predictions as discussed above

We also note that the present collaboration builds on a previous SIN-Virginia effort to determine $\Delta = m_+ - m_0$ precisely [Cra-86, -88], which in effect eliminated the experimental contribution to the overall uncertainty in the $\pi\beta$ decay rate.

2. DESCRIPTION OF THE EXPERIMENT

2.1. **Introduction: choice of the experimental technique**

Because of the very small branching ratio for the decay $\pi^+ \to \pi^0 e^+ \nu$ ($BR \approx 1.0 \times 10^{-8}$), and the high required measurement precision, the following requirements must be met by the experimental apparatus:

(i) ability to handle high event rates,

(ii) large solid angle coverage and efficiency for π^0 detection,

(iii) very good energy and timing resolution for efficient suppression of background events in hardware, and

(iv) accurate calibration and low systematic errors.

The background processes which must be distinguished from $\pi\beta$ events include (branching ratios in parentheses):

$$
\begin{array}{lll}
\pi^+ \to & \mu^+\nu & (1.0), \\
 & e^+\nu & (\sim 1.2 \times 10^{-4}), \\
 & \mu^+\nu\gamma & (\sim 1.2 \times 10^{-4}), \\
 & e^+\nu\gamma & (\sim 5.6 \times 10^{-8}), \\
\mu^+ \to & e^+\nu\overline{\nu} & (1.0), \\
 & e^+\nu\overline{\nu}\gamma & (\sim 0.014), \\
 & e^+\nu\overline{\nu}e^+e^- & (\sim 3 \times 10^{-5}),
\end{array}
$$

as well as their accidental coincidences.

Subsequent to our submission of the original preliminary proposal (PSI letter of intent R-89.01.0), we were encouraged by the BV to examine all feasible experimental designs optimizing for highest rate and lowest systematic uncertainties, disregarding costs in the analysis. As outlined in Section 1., the level of accuracy of ~0.1 – 0.3% is of particular physical significance, given the theoretical uncertainties and the state of nuclear Fermi decay results. We have considered both decay in flight and at rest, and review our findings below.

2.1.1. Decay in flight

At first glance, this appears to be the more attractive technique of the two. Although high pion beam intensity is required, the average raw rates in the detectors are low, about two orders of magnitude lower overall than in the stopped experiment. In principle, one can perform the measurements with both $\pi^+$and π^-beams, which provides a useful systematic check. Furthermore, this technique measures the $\pi\beta$ decay rate fairly directly, detecting a certain number of decays in a known amount of pion proper time.

A thoroughly researched proposal (SIN number R-82-01.1, [Bor-82]) for an in-flight measurement was submitted to the SIN BV by the Bern group, and was taken into account in our analysis, as was the most recent measurement of the $\pi\beta$ decay rate by McFarlane *et al.* [McF-85]. We have examined ways in which both of these setups could be improved given the intervening developments of detector techniques.

Upon closer analysis, however, important drawbacks to the in-flight technique become apparent, limiting the possible improvements over [McF-85] and [Bor-82]. We shall discuss them below in the order of their importance.

(a) Normalization

In-flight detection is an absolute measurement and requires absolute counting of beam pions, as well as an absolute determination of the detector acceptance, efficiency, and pion proper time in the decay region. To our knowledge, no scheme has been demonstrated to date to achieve an accuracy significantly better than 1% in counting beam pions at intensities of $\sim 10^8$ s^{-1} and momenta of >400 MeV/c. To achieve this with uncertainties of $\sim 10^{-3}$ appears to be well outside present experimental capabilities.

A way around the problem of absolute normalization above, would be to use another well measured pion decay channel for normalization. The only option is to choose $\pi \to e\nu$. This would eliminate the need to count beam pions, but would require precise knowledge of the acceptance/conversion efficiency for both $\pi\beta$ and $\pi e\nu$ processes, as well as a selective and bias-free single-arm trigger for the latter decays. The acceptances for $\pi\beta$ and $\pi \to e\nu$ decays differ by about a factor of 2 for reasonable geometries (cf. Figure 1), so that uncertainties do not cancel out in the ratio. Systematics of the absolute determination of the acceptance for $\pi\beta$ events are discussed below. It is worth noting here that the outer boundary region of the detector (i.e., large radii in Figure 1) is relatively more important for the $\pi e\nu$ acceptance in a detector of cost-effective size.

(b) Acceptance

An absolute determination of the effective acceptance of a π^0 shower detector at the desired level of accuracy is difficult due to edge effects. Even an infinitely large "wall" shower detector must have a sizable hole to let the beam and Michel electrons through. This edge region, however, contributes most significantly to the total acceptance. This is shown quantitatively in Fig. 1 for a setup with a 3 m decay region, using pions of 450 MeV/c. Shown in the figure is the radial dependence of the in-flight detector acceptance for $\pi\beta$ and $\pi \to e\nu$ shower events. For a reasonable geometry, a radial uncertainty of 1 cm in the γ fiducial area translates into a $\sim$3% uncertainty in the total acceptance. As we demonstrate in Section 2.9., it is possible to model the physical processes occurring in electromagnetic showers with reasonably high accuracy. However, the spatial resolution of conversion points in a detector of a reasonable geometry is limited to about 1 cm or more. This makes the Monte Carlo calculation of the absolute acceptance critically dependent on the detailed knowledge of the beam geometry.

In order to improve spatial resolution of the conversion points, one can use thin converter planes, and a hodoscope (e.g., wire chambers) to reconstruct conversion vertices. Using converter planes thinner than 1 radiation length followed by MWPC's for shower tracking can give linear resolution of order of 1 mm; using drift chambers can improve the resolution to the level of several hundred microns, which is more than sufficient for the purpose discussed here. In order to restore a reasonable total detection efficiency, it is necessary to use several such sandwiches of converter planes and charged particle detectors.

While improving vertex reconstruction, the use of converter planes and tracking detectors introduces several complications. Firstly, absolute normalization requires that the conversion efficiency of each converter-wire chamber sandwich be calibrated to the desired accuracy. This includes both the converter efficiency (which depends on the photon angle of incidence, and thus on beam geometry), and the track reconstruction efficiency (which depends on the algorithm used besides the wire chamber instrumental efficiency). Although a good design can minimize the mentioned dependences, such a calibration to $\sim 10^{-3}$ accuracy appears to be beyond the presently available techniques . Secondly, breaking up the shower detector affects unfavorably the energy resolution, which is more critical at 450 MeV/c than for decays at rest. Additionally, as the depth of the shower detector is increased to accommodate vertex reconstruction detectors, showers spread over a larger volume, which effectively reduces acceptance in the beam hole region, where it counts the most.

(c) Triggers

Because pion decays occur in flight over an extended decay region, there is no unique correlation between the shower energy and the coordinates of the conversion point. If the $\pi e\nu$ decays are chosen for normalization, an energy-angle cut is required for their identification, so that placement of a tracking detector in front of the calorimeter is necessary. In a realistic experimental situation, the tracking accuracy, and thus the energy-angle cut efficiency, will be limited by beam size, divergence and momentum distribution. On the other hand, energy resolution in the shower calorimeter is important for the separation of both $\pi\beta$ and $\pi e\nu$ decays from the Michel and other backgrounds. It is needless to say that the π–μ energy separation of about 30 MeV is resolved more easily for $\sim$60 MeV showers (decays at rest) than for $\sim$300 MeV showers (decays in flight).

(d) Rate limitations

Dynamic constraints on feasible $\pi\beta$ data rates are considerable, despite the overall low raw detector rates. Due to a high kinematic boost of all events, their energy separation in the detector is difficult. Particularly troublesome are the radiative backgrounds $\pi \to e\nu\gamma$ and $\mu \to e\nu\overline{\nu}\gamma$ (see [Bor-82]). Unlike the stopped pion experiment, the effective detector duty factor for in-flight measurement is $\sim$1/20 given the PSI beam structure. This exacerbates the suppression of accidentally coincident backgrounds like $(\mu \to e\nu\overline{\nu})^2$. In order to suppress them by a time-of-flight cut, a long beam-line is needed (60 m in proposal R-82.04.1), which reduces the total available pion beam intensity. These factors combine to limit the feasible $\pi\beta$ rates to a level close to that of proposal R-82.04.1, i.e., $\sim$0.004 s^{-1}. As is seen in Figure 1, enlarging the shower detector does not help at all beyond a certain point because the size of the hole determines the total acceptance for $\pi\beta$ events and not the outer boundary.

(e) Size and cost of the detector system

Figure 1 gives a good indication of the size requirements for an in-flight decay detector. Considering only the shower calorimeter (the most expensive part), and assuming the use of pure CsI as in the stopped experiment, a simple calculation yields a volume of upwards of 1.5×10^6 cm^3, or about \$4 M. This is more than four times the volume of a corresponding stopped-decay shower calorimeter (see Section 2.7.). Of course, certain other associated costs (readout, electronics, etc.), scale with the calorimeter volume, as well.

2.1.2. Decay at rest

Detection of pion decays at rest has the obvious disadvantage of having to accept in the detector all of the Michel positrons from muon decays in the target. Furthermore, one measures a branching ratio from which the decay rate must be evaluated using the pion lifetime.

However, there is much to be gained by making the stopped experiment into a relative rather than an absolute measurement by normalizing to the $\pi \to e\nu$ decay events. The detector acceptance and response to the $\pi e\nu$ events are found to be very similar to the $\pi\beta$

events, so that the differences in systematic uncertainties are small and manageable. This is due to the fact that the photons from $\pi\beta$ decays and positrons from $\pi \to e\nu$ decays produce very similar showers. In addition, the corrections to detection efficiencies for both decays are small and very well understood. These important points will be discussed individually and supported by detailed Monte Carlo calculations in Section 2.9.

Our design furthermore calls for a highly segmented shower detector, sufficiently removed from the source of decays, made up of a very fast and luminous shower scintillator material (see Section 2.7. for details and justification). By satisfying such requirements it is possible to design a setup with a surprisingly high rate capability. Identification of $\pi\beta$ events then relies on good energy and timing resolution and moderate spatial resolution of the shower calorimeter. Our proposal is based on these principles.

A natural remedy for the high Michel rate would be to place the entire detector inside a strong magnetic field to sweep away the positrons. This option, however, alters the systematics of both $\pi\beta$ and $\pi e\nu$ events in such a way that they are no longer similar, nor can they be related in a precise fashion.

2.1.3. Conclusions

Our conclusion is that a relative measurement rather than an absolute one is far preferable, particularly if it allows a higher rate of data taking than the 0.004 s^{-1} mentioned above. Simply put, it is too hard to control the systematics with $\sim$0.1% accuracy in an absolute measurement of a rare process occurring with 10^{-8} probability. We find that, given the present state of experimental techniques, a relative measurement of the pion beta decay branching ratio at rest, as outlined in the following sections, represents the most promising and cost effective way to improve the accuracy of the present $\pi\beta$ decay rate.

2.2. **Outline of the experimental method**

For the above stated reasons, measurements will be carried out in a stopped-pion experiment. The experimental apparatus will have the following main components:

(i) beam counters and an active target to stop the pions,

(ii) a high-resolution highly segmented fast shower calorimeter surrounding the active target in a near-spherical geometry with an opening for beam entry and a symmetric one for light readout from inner detectors,

(iii) a cylindrical multi-wire proportional chamber for charged particle tracking surrounding the active target inside the shower calorimeter,

(iv) a segmented fast veto counter surrounding the MWPC, inside the shower calorimeter, and

(v) cosmic ray veto counters around the entire apparatus.

A simplified schematic layout of the experimental apparatus is shown in Figure 2.

Beam pions will be identified by means of timing and pulse height information in the beam telescope counters including the active target at low rates. Each pion stopping in the target will initiate a delayed beam pion gate (DPG), timed so as to avoid inclusion of prompt strong-interaction events, i.e., delayed by 10 ns and not longer than 100 ns. Pion beta decays will be registered during the delayed pion-stop gate through coincident detection of two γ

rays (from $\pi^0 \to \gamma\gamma$) in the shower calorimeter. We do not plan to detect the positron pulse in the pion stop counter, except in the early runs with very low pion rates. Normalization will be performed using events collected during $\pi \to e\nu$ triggers. These will consist of single-arm well localized individual showers with energy deposition exceeding a threshold set at 55 MeV or higher, during the DPG. Due to the large discrepancy in branching ratios, the $\pi e\nu$ triggers will be prescaled. As for the $\pi\beta$ triggers, a good event is not allowed to be followed closely by a beam particle in order to avoid pile-up caused by a prompt strong-interaction event. The triggers will be discussed in more detail below.

Crucial for obtaining a reasonable trigger rate are the spatial, energy and time resolution provided by a highly segmented shower calorimeter detector system, which make possible clear selection of individual showers whose energy lies above the Michel background. In many respects the proposed detector system resembles the SLAC Crystal Ball [Ore-82]. The fast veto and MWPC's are not planned to be initially included in the trigger, although that may become necessary in the second phase of the measurements discussed below.

The $\pi\beta$ decay rate is given by the simple ratio:

$$\frac{1}{\tau_{\pi\beta}} = \frac{1}{\tau_\pi} \cdot BR_{\pi\beta} = \frac{1}{\tau_\pi} \cdot \frac{BR_{\pi\to e\nu} N_{\pi\beta}}{(N_{\pi e\nu} \cdot f_{presc}) \cdot BR_{\pi\to\gamma\gamma}} \times corrections, \tag{2.1}$$

where τ_π is the pion lifetime, the N's represent the respective numbers of good $\pi\beta$ and $\pi e\nu$ events, and f_{presc} is the prescale factor for the $\pi e\nu$ trigger. Besides the usual effects associated with background subtraction, the above corrections include ratios of the following quantities for the two triggers, respectively:

- shower detector acceptances,
- livetime corrections,

as well as:

- neutral shower self-vetoing due to back-splash,
- in-flight annihilations of positrons in the target and charged particle detectors,
- leak-through of γ's from π^0 decay which do not deposit any energy in the calorimeter,
- instrumental inefficiency of the MWPC and fast veto counters, and
- acceptance corrections due to finite size of the pion stopping distributions.

Detailed Monte Carlo simulations have shown that each of the above ratios and correction factors represent effects differing by a few percent from unity, and that we can calculate and/or measure the associated uncertainties at the level of better than a factor of 10 lower than the effects themselves (see Section 2.9. for details). In this way systematic uncertainties can be reduced to the level of several per mill, without the need to make any absolute measurements initially. The remaining requirement is to construct triggers selective enough, as well as free of bias, capable of sustaining high rates.

We propose to make the measurements in two stages. The goal for the first stage will be to build, set up, and bring up to full speed the detector system, and finish running at typically $\sim 1\times 10^6$ or more stopped pions per second. Under those conditions we would obtain $\pi\beta$ results with statistical uncertainties under 0.5%. Taking into account the soon forthcoming $\pi \to e\nu$ experimental branching ratio from the Bern-SIN collaboration expected to be accurate to $\sim$0.3%, and the other systematic uncertainties, we should end up with a result in the range of 0.5 – 0.6% accuracy. This would represent a significant improvement in itself.

The next step in precision will require a new measurement of the $\pi \rightarrow e\nu$ decay branching ratio (improving the precision to ~0.1%), and subsequent $\pi\beta$ measurements with an improved trigger at a higher stop rate, $\sim 5\times 10^6$ s^{-1}. At this rate, given 2×10^7 s of beam time, we would obtain ~0.15 – 0.2% counting statistics, which would lead to an overall uncertainty in the range of 0.2 – 0.3%.

In this proposal we wish to demonstrate the feasibility of such precise $\pi\beta$ decay measurements. We shall not discuss here the improved measurement of the $\pi \rightarrow e\nu$ branching ratio. By virtue of being four orders of magnitude more probable, we feel that this decay mode is inherently easier to measure than the $\pi\beta$ decay.

2.3. The π^+beam

Requirements on the beam are as follows:

(i) small beam spot size, ~1 cm diameter,

(ii) small stopping depth, ~1 cm,

(iii) minimal contamination with μ^+ and e$^+$ ($< 10\%$),

(iv) possibility to cut out muons and electrons by their time of flight,

(v) stopping rate of $\sim 0.1 - 2 \times 10^6$ s^{-1}.

In our test run in 1989, before the shutdown of beams at PSI, we studied the pion beam properties and contamination in the πE1 area as a function of momentum. The results are summarized in Figure 3. Several facts are evident. There will be enough stopping pion rate for our needs after the PSI accelerator upgrade, even as low as 100 MeV/c. The e/π and μ/π contaminations increase at lower momenta, particularly the former which reaches values of the order of 10. This cannot be tolerated by our trigger since it would induce inordinate dead time and background counts. We therefore need to use an electrostatic separator in order to remove most of the positrons from the beam.

2.4. The beam telescope counters and active target

A beam telescope and an active target will be placed in the beam in order to define the stopping particle (see Figure 2). All will be made of plastic scintillator. Pulse height information in each counter will be recorded throughout the run on a prescaled basis for π's, μ's and e's separately, so that their signatures are monitored. Appropriate Pb shielding will be installed in order to shield the calorimeter from prompt background events induced in the beam telescopes and upstream.

As has been pointed out, the experiment relies on an accurate comparison of the branching ratios of two decay modes, (1)$\pi^+ \rightarrow \pi^0 e^+ \nu$ and (2)$\pi \rightarrow e\nu$. While the energies of the γ's from the π^0 decay in reaction (1) and the e^+ in reaction (2) are quite similar, there are slight differences due to the π^0 recoil. This recoil ranges up to 75 keV, and averages 54 keV. Due to the recoil, the two γ rays from π^0 decay are not exactly collinear. Their relative directions deviate from a straight line by at most 3.8°, on average by 3.2°. The deviations from collinearity induce small differences in the acceptances for decays (1) and (2). These differences will have to be accounted for in a precise Monte Carlo simulation of the experiment. Such a simulation will require knowledge of the stopping distribution.

Since it is not feasible to measure the stopping position event by event, we will have to settle for separate measurements of the z and r distributions. The z-distribution will be obtained from a measurement of the pion range curve. Since the fields in the bending magnets are tightly controlled, and we will use a feedback mechanism developed by M. Daum for more restrictive control, it will be sufficient to verify the range distribution only occasionally.

We plan to determine the r-distribution with an active target consisting of a bundle of 69 $3{\times}3$ mm^2 square scintillating plastic fibers surrounded by an 8-element guard ring, as shown in Figure 4. The range of 100 MeV/c pions in scintillator is 40 mm, and we plan to make the fibers 40 mm long, forcing the pions to stop in the target volume with a preceding scintillator telescope consisting of two plastic scintillators of 5–10 mm total thickness.

The active target will be coupled through fiber optics light guides to individual small photomultipliers. In view of the limited energy resolution of a fiber target, it will probably not be possible to use the 77-element active target during the entire run. We will therefore design and construct a simpler active target, combining rate handling ability and good energy resolution, to be used during most of the running time. It will be replaced with the 77-element target as often as advisable. Care will be taken to make the two targets as nearly identical as needed in position, construction, and material.

2.5. **Charged particle tracking detector – MWPC's**

The primary need for a tracking detector in the experiment is due to the $\pi \to e\nu$ decay trigger. Whereas individual Michel events can be discriminated from the positrons from $\pi e\nu$ decays, in a high-rate measurement, accidentally coincident Michel events will give rise to a substantial background under the $\pi \to e\nu$ peak. The power of multiple shower resolution of the calorimeter is limited. Given the calorimeter design size, geometry and segmentation, this resolution is expected to be $\sim$0.004 of 4π in solid angle (see section 2.7. for more details on shower profiles). For suppression of accidental Michel coincidences occurring with high pion stopping rates ($5\ \times 10^6$ s^{-1}), higher double-event resolution is required. The limit on the useful resolving power is set by the fraction of in-flight annihilations of Michel positrons in the target, which is about 2% for the target of 25 mm radius. It therefore does not pay to provide suppression factors beyond $\sim 10^{-3}$.

The following constraints had to be met in the design of the tracking detector, besides the above double-track resolution:

- low mass, in order not to initiate showers from π^0 decay γ rays,
- high efficiency, of order $1 - 10^{-3}$,
- high rate capability, up to 10^7 minimum-ionizing particles (MIP) per second,
- stable operation and good radiation hardness,
- cylindrical geometry.

We considered several design options: (a) MWPC's, (b) scintillating fiber hodoscopes, and (c) Si microstrip arrays. Of all these, the MWPC's provided the best combination of required qualities listed above. In addition, wire-chamber technology is the most mature and reliable among the available choices.

The wire-chamber design we selected happens to be very similar to that of the CP-LEAR PC2 [Bas-85, Ket-90]. It is a pair of cylindrical chambers, each with one anode wire plane in the z direction, and two cathode strip planes in stereoscopic geometry. The main parameters are:

	Ch 1	Ch 2
active length, mm	350	540
inner radius, mm	42.5	107.5
wire layer radius, mm	60	120
outer radius, mm	70	128
number of wires	192	384
strip width, mm	∼3	2
no. of outer/inner strips	2x64/2x64	224/224
half gas gap, mm	2.5	2.5
chamber wall thickness, RL	0.0013	0.0019.

The thickness of the entire MWPC assembly to γ rays is about 3×10^{-3} radiation lengths, negligible compared to the thickness of the active target (0.06 RL) which dominates in the path of particles to the calorimeter. The expected double track resolution should be ∼2.5 mm or better, leading to an additional suppression factor for accidental Michel coincidences of about 6×10^{-3} over the calorimeter double shower resolution.

Similar chambers have been built and successfully operated by the Dubna group in the past.

2.6. Fast veto counters

In order to provide efficient identification of charged particle-induced events, it necessary to detect them with good timing resolution. For this reason the wire-chamber detector will be followed by a fast thin plastic scintillator veto counter in the shape of a cylindrical shell (see Figure 5). Its main parameters are:

outer radius: 140 mm

thickness: 5 mm (0.01 RL)

active length: 550 mm

number of modules: 20 (interleaved edges)

readout: longitudinal, both ends, photomultiplier tubes.

Design of this detector was determined by the requirements to provide reliable MIP identification with minimum thickness, and with granularity consistent with that of the shower calorimeter. The need for modularity is dictated by the desired stopping rate.

The energy deposition spectrum in the plastic veto (PV) counters calculated using the computer program GEANT for Michel events is shown in Figure 6. We have performed Monte Carlo simulations of light collection probabilities for the veto strips, and found satisfactory uniformity. The chosen PV thickness allows for a good separation of the MIP peak, and therefore of neutral and charged tracks, even after folding in the light collection statistics and nonuniformity. The selected charged particle threshold is denoted by an arrow in Figure 6, and has been used in evaluating the results of subsequent simulations, which are presented below. From past experience, we expect the instrumental efficiency of these counters to be 0.99 or better. As stated above, however, Michel positron conversions into neutrals which occur at the ∼2% level, limit the overall efficiency of suppression of neutrals.

Design is evolving. We are presently investigating having the elements cast, and are continuing design studies.

2.7. Shower calorimeter

The shower calorimeter lies at the heart of the experiment. We have made considerable progress on its design since the submission of our preliminary proposal in December 1988. In that proposal we argued in favor of using the hyperpure CsI as the calorimeter material, and listed its properties as they were known then [Kub-88]. In a series of laboratory tests in Virginia and PSI, and finally in beam at PSI, we came to the following conclusions.

(1) The attenuation length for its own scintillation light is quite long, of order of 1 m for good material, unlike the 35 cm value reported in Kub-88. This enabled us to redesign the calorimeter in a "tower" geometry, with single-ended detector readout, which is inherently more favorable for high-rate measurements.

(2) Timing resolution in large crystals of good quality (with over 100 photoelectrons/MeV) is $\sigma \approx 400$ ps/phototube, and ranges up to 600 ps for crystals with 50 or fewer photoelectrons/MeV.

(3) Large crystals, subtending 0.4 sr operated very quietly in realistic conditions with beam. As expected, signal clipping did not impair detector resolution.

These points are illustrated in Figure 7 which summarizes the results of our development run of November 1989. In this run, we stopped a 175 MeV/c π^+parasitic beam in an active plastic scintillator target in the πE1 area. The target was viewed by two arms, an array of 7 large CsI hexagonal modules on one side, and a NaI detector on the other. The two detectors were subtending matching solid angles at 180°. Both arms had thin plastic vetos in front of the crystal detectors.

Unfortunately, the November 1989 development run took place under severe time constraints imposed by the pending long shutdown of the PSI ring accelerator on the one hand, and by the very late delivery of CsI crystals by Bicron Corporation. As it turned out, the CsI modules delivered by Bicron were sub-standard in their performance, which resulted in energy and timing resolution of our development run poorer than what we found in previous tests of good pure CsI pieces. In addition, the time constraints limited our running time and counting statistics. All of those deficiencies are apparent in Figure 7. However, the measured signal, background and trigger rates conformed closely to our predictions, verifying the basic validity of our approach.

Figure 7(a) shows the relative timing spectrum obtained between a CsI block and the target counter (plastic scintillator), with a FWHM of 1.3 ns. The photomultiplier tubes used for CsI light readout were EMI model 9821QB (quartz window), with a nominal rise-time of 2.1 ns. Previously, the same photomultiplier tubes coupled to good pure CsI detectors of similar size yielded 1.1 ns FWHM resolution between two crystals in laboratory tests at UVa with a ^{60}Co source. This is sufficient to meet the demands of our experiment. For crystal modules satisfying our specifications we expect even better timing for the typical in-beam events which are considerably more energetic than the ^{60}Co photons.

Figure 7(b) shows the spectrum of the summed NaI and CsI energies, detected inside an 80 ns wide gate following a valid pion stop by 10 ns. The spectrum shown includes showers registering as both charged and neutral in the plastic veto counters. The energy conversion factor is about 3 channels/MeV. The portion of the spectrum below about 104 MeV (ch. 310) was prescaled by a factor of about 100. The pion stopping rate was 2×10^5 s^{-1}. The recorded spectrum is dominated by accidental coincidences of Michel positrons in the NaI and CsI arms. The observed shape, as well as total rate, are in very good agreement with our simulations. The observed rate above about 100 MeV is very low for non-prompt events, as shown in Figure 7(b).

Figure 7(c) displays the same quantity (sum of CsI and NaI arm light outputs) for the unprescaled energetic events ($>$ 100 MeV), satisfying the condition that both showers be neutral (no plastic scintillator veto counter firing for either arm). A well defined $\pi\beta$ peak emerges at the correct energy, after these cuts are imposed. Due to the already mentioned time constraints, the statistics in Figure 7(c) is poor; it reflects only about 4 shifts of running. It is, however, very gratifying that the observed peak is clean, and the number of counts corresponds very well to the branching ratio of 1×10^{-8}.

The geometry of the shower calorimeter was chosen following these guidelines:

- high rate-handling ability – low pile-up and dead time;
- high energy resolution for Michel event suppression;
- optimization of light collection efficiency for modules;
- uniform coverage of solid angle by detector modules for even distribution of counting rate;
- maximum economy of different module shapes compatible with above requirements.

All of these requirements were best met in a nearly-spherical geometry obtained by the geodesic triangulation of an icosahedron. In this respect, our design bears similarities to the SLAC Crystal Ball [Ore-82]. However, in order to enhance light collection efficiency, we opted for truncated hexagonal and pentagonal pyramids rather than triangular pyramids of the Crystal Ball. Here are the main properties of the shower detector geometry:

inner radius: 260 mm

outer radius: 480 mm

average thickness: 12 RL

number of modules: 240

active detector modules: 220

edge veto modules: 20

total solid angle: $\sim$0.77 of 4π sr

average solid angle subtended by a detector module: $0.004 \times 4\pi$ sr

geodesic breakdown: Class II

number of different modules: 5 (4 hexagonal and 1 pentagonal truncated pyramids)

volume of CsI: about 346,000 cm^3

expected optical nonuniformity: 2.5% FWHM or better

readout: 50 mm phototubes with quartz window (likely EMI 9814QB)

The basic detector geometry, its dimensions and granularity were chosen on the basis of detailed Monte Carlo simulations of shower development performed using the codes EGS4 and GEANT, as follows.

Thickness of the calorimeter: GEANT calculations of the shower calorimeter response to $\pi\beta$ decay events are shown in Figure 8 as a function of the outer radius of the CsI detector. Curves shown include smearing due to light collection statistics and nonuniformity. The thicknesses considered correspond to 10, 12 and 14 radiation lengths, respectively. Shown in the same figure is the steeply rising accidentally coincident Michel background, which sets a lower limit for acceptable $\pi\beta$ shower energies at about 110 MeV or higher. All three detector thicknesses yield a reasonable efficiency, varying between 0.70 (10 X_o) and 0.75 ($14X_o$). The thicker geometries give, however, better energy resolution which is important in differentiating the $\pi\beta$ peak from the underlying broad backgrounds (see Figure 10). The volume, and therefore cost, increase also with the cube of the outer radius. We believe that a reasonable compromise is found with $12X_o$, which requires about 110,000 cm^3 (almost \$300,000) less CsI than the $14X_o$ solution.

Detector granularity is decided by considering the geometry of shower spreading. Figure 9 shows the mean energies and the associated FWHM's of distributions of shower energy deposited inside conical fiducial volumes of our shower calorimeter. To obtain these curves, we ran GEANT calculations of shower propagation inside our detector, keeping track of the location of energy deposition at each step. The original particles (70 MeV γ's and e^+'s) were thrown from the center of our stopping target, and were tracked throughout the detector volume. The shower energy deposition in CsI was histogrammed into 1° conical bins concentric with the direction of the original particle's momentum. Thus, the abscissa in Figure 9, labeled θ_{cut}, corresponds to the half-angle of the opening of the conical fiducial volumes. It is seen that

(a) the mean, as well as the width, approach saturation inside a cone of about $10-12^\circ$ half-angle, and

(b) shower profiles for events initiated by γ's and positrons are very similar, particularly in the saturation of deposited energy. This point is especially significant for controlling the systematic errors associated with the normalization to the $\pi \to e\nu$ decays (cf. Section 2.9.).

Our choice of granularity is such that if hit centrally, any module will contain about 90% of the shower energy. At most three modules should receive significant portions of a single particle's shower energy. Due to this sharing, the spatial reconstruction of the shower centroid will be a fraction of the solid angle of an individual detector element (0.004 of 4π). In this way, clusters of 7 elements provide an excellent trigger element, and clusters of 3 elements are also satisfactory. In this respect the stopped experiment is favored over the in-flight measurement involving more energetic showers.

Minimizing dead time and pile-up has also been a concern in the design. The present granularity will keep the dead-time due to pile-up under the percent level. We plan to clip the signals, as necessary, in order to further reduce module dead time. Identification of pile-up in the shower detector modules will be done by using early and late gates for digitization of charge for each of the phototubes, in addition to the usual in-time gate. This technique has given good results in our tests.

Light collection Monte Carlo calculations indicate, as is to be expected, nonuniformities in light response due to geometric effects of the slanted edges. We plan to paint the forward surfaces with a diffusely reflecting paint. Another way to achieve uniformity is by grading the forward surfaces; this option will also be considered. The modules will be optically isolated from each other.

The high temperature coefficient of CsI dictates that the calorimeter be kept enclosed in a temperature-controlled environment. In addition, because of its slight hygroscopicity and long running, this atmosphere needs to be air-conditioned. An air temperature-control device was used in experiment R-82-04.4, the measurement of the branching ratio $\pi \to e\nu$ $/\pi \to \mu\nu$, and could be used in our experiment with minor modifications.

Prior to assembly, all modules must be examined for optical uniformity. The most reliable way of accomplishing this is to use cosmic ray tomography. At the University of Virginia we are in the process of putting together a facility capable of tomographing a number of modules at once.

2.8. **Trigger rates**

As was discussed in Section 2.2., there are two main data triggers, the $\pi\beta$ and $\pi e\nu$. Building blocks of the triggers are overlapping groups of seven (on average) modules. Each group has associated with itself a symmetric group in the opposite hemisphere. The two triggers are only enabled during a delayed pion gate (DPG). In addition to the above two triggers, there will also be a cosmic ray trigger, a more delayed trigger (DPG') and a calibration type of event. We shall discuss them briefly below. The two main triggers have been extensively analyzed with the help of Monte Carlo simulations (codes EGS4 and GEANT have been used). We cannot present all of the details here, but will mention the main characteristics, potential problems, and will summarize the rates in tables.

The $\pi\beta$ trigger requires a coincidence of two showers within 20 ns, inside a valid DPG, each exceeding a threshold of $\sim$55 MeV, occurring in two diametrically opposed trigger groups. Due to the very high threshold, only 4-fold and higher order accidental Michel coincidences will fire this trigger. This leaves $\pi \to e\nu\gamma$ as the sole competing channel in this trigger. The relevant rates are summarized in Tables 1 and 2, for the stopping rates of 1×10^6 and $5 \times 10^6 \pi$/s, respectively. Figure 10 shows the relative energy distributions of the $(\mu \to e\nu\nu)^2$ and $\pi \to e\nu\gamma$ events in this trigger for the higher pion stopping rate. In order that we may see the yield from the $\pi \to e\nu\gamma$ decay, its spectrum shown in Figure 10 does not include a cut on neutrals in the plastic veto counter. Once applied, this cut reduces the $\pi \to e\nu\gamma$ contribution by a factor of about 100, leaving a very clean $\pi\beta$ signal.

The $\pi e\nu$ trigger is a single-arm trigger, and therefore much more susceptible to accidental coincidences of Michel events. In fact, as Tables 1 and 2 reveal, at the higher stopping rate the $\pi \to e\nu$ events ride on a substantial background of accidental Michel coincidences. While there are no problems in cutting out the background off-line, care must be taken that the trigger remains sufficiently restrictive, without introducing bias. For that reason we are considering implementing in the second stage of the experiment a fast pile-up rejection circuit, used by members of this collaboration in the experimental search for the heavy neutrinos [Dau-87], as well as a software pretrigger involving MWPC information. We can also reduce the trigger group size from 7 to 3 modules in order to enhance selectivity for single-arm events.

The Michel backgrounds will be understood by measuring separately very late events with respect to the pion stop time. Events accumulated in the DPG' gate will, therefore, serve to get a better shape of the energy distribution and rate for these processes.

A special on-line energy calibration procedure will be implemented also. At its heart will be a laser whose light will be channeled to all of the calorimeter detector modules, and

Table 1. Main trigger and background rates at the beam rate of $r_{\pi stop} = 1 \times 10^6 s^{-1}$.

Process	Rate in trigger (s^{-1})	Energy, time cuts	Track and shower cuts	Prescale factor	Final rate (s^{-1})
		$\pi\beta$ trigger			
$\pi^+ \to \pi^0 e^+ \nu$	0.005	1	1	1	0.005
$\pi^+ \to e^+ \nu\gamma$	4×10^{-4}	1	10^{-2}	1	4×10^{-6}
$(\mu \to e\nu\nu\gamma)^2$	1×10^{-4}	$< 10^{-1}$	10^{-5}	1	$< 10^{-10}$
$(\mu \to e\nu\nu)^4$	1×10^{-5}	10^{-2}	$\leq 10^{-6}$	1	10^{-13}
$(\pi \to e\nu)$ $\times(\mu \to e\nu\nu)^2$	1.9×10^{-5}	0.013	$\leq 10^{-6}$	1	$\leq 10^{-12}$
		$e\nu$ trigger			
$\pi^+ \to e^+ \nu$	63	1	1	10^2	0.63
$(\mu \to e\nu\nu)^2$	30	0.1	7×10^{-4}	10^2	2×10^{-5}
$(\mu \to e\nu\nu)$ $\times(\mu \to e_C\nu\nu\gamma)$	0.5	0.1	0.2	10^2	10^{-4}

Table 2. Main trigger and background rates at the beam rate of $r_{\pi stop} = 5 \times 10^6 s^{-1}$.

Process	Rate in trigger (s^{-1})	Energy, time cuts	Track and shower cuts	Prescale factor	Final rate (s^{-1})
		$\pi\beta$ trigger			
$\pi^+ \to \pi^0 e^+ \nu$	0.023	1	1	1	0.023
$\pi^+ \to e^+ \nu\gamma$	0.002	1	10^{-2}	1	$\sim 2 \times 10^{-5}$
$(\mu \to e\nu\nu\gamma)^2$	0.0025	$< 10^{-1}$	10^{-5}	1	$< 3 \times 10^{-9}$
$(\mu \to e\nu\nu)^4$	0.006	10^{-2}	$< 10^{-6}$	1	$< 10^{-10}$
$(\pi \to e\nu)$ $\times(\mu \to e\nu\nu)^2$	2×10^{-3}	0.01	$\leq 10^{-6}$	1	$< 10^{-10}$
$(\mu \to e\nu\nu)^3$ $\times(\mu \to e\nu\nu\gamma)$	1×10^{-5}	10^{-2}	10^{-6}	1	$\sim 10^{-13}$
		$e\nu$ trigger			
$\pi^+ \to e^+ \nu$	270	1	1	10^3	0.27
$(\mu \to e\nu\nu)^2$	2200	0.1	0.2×10^{-3}	10^3	$< 10^{-4}$
$(\mu \to e_C\nu\nu)$ $\times(\mu \to e\nu\nu)$	33	0.1	0.2	10^3	$\sim 7 \times 10^{-4}$
$(\mu \to e\nu\nu)$ $\times(\mu \to e\nu\nu\gamma)$	3	0.2	0.2	10^3	$\sim 10^{-4}$
$\pi \to e\nu\gamma$	0.003	1	0.2	10^3	$< 10^{-6}$
$(\mu \to e_C\nu\nu)^2$	0.2	0.1	10^{-3}	10^3	$< 10^{-7}$

fired periodically in the absence of beam, providing on-line energy calibration of the entire detector system. This concept is being developed at the University of Virginia presently.

2.9. Systematics and calibrations

The main sources of systematic uncertainties have been identified in Section 2.2. Apart from the livetime corrections (which will be small and subject to detailed experimental determination), the size of the systematic uncertainties is determined by the accuracy of our calculation of:

(a) distribution of deposited energy, as well as geometry of shower spreading,

(b) shower leakage through the back of the calorimeter,

(c) neutral and charged particle back-splash from showers; the latter is particularly important as it introduces self-vetoing of γ-induced showers, and

(d) in-flight annihilation of positrons inside the target, air, and veto detectors, leading to failure to identify the original particle as charged.

We have carefully examined the reliability of presently available shower codes in modeling all of these processes. At present there exist three fully versatile shower simulation codes: ITS (Tiger), EGS4, and GEANT. In order to minimize any bias or inaccuracy potentially introduced by the purely geometrical portions of these codes which can be tested separately, we undertook a comparison using a simplified planar detector geometry. Our setup consisted of a target counter, and a thin plastic veto (PV) counter followed by 12 radiation lengths of CsI. By appropriately choosing the origin of our primary particles (70 MeV γ's or positrons), we could address each of the points (a) - (d) above. Our main findings follow, and are illustrated in Figures 11 and 12.

After careful adjustment of tracking parameters to reflect a very fine track step size and low tracking cut-offs for all shower particles, each of the three codes showed convergence to an asymptotic result. It is even more gratifying that the final results of the three codes show remarkable agreement, which is absent in coarse calculations. We have to stress that although all three programs (ITS, EGS4 and GEANT) are designed to describe the same physical processes, there exist modeling differences among them, as well as the use of different computational algorithms.

Shower spreading profiles calculated using GEANT have been discussed in Section 2.7. and presented in Figure 9. The shower deposition mechanism in all three codes is nearly identical. Top panel in Figure 11 shows the results for a 70 MeV γ-induced shower line-shape in CsI as calculated by GEANT, ITS and EGS4. In the energy region of interest, above 50 MeV, the agreement between the calculated line-shapes is excellent. The integrated detection efficiencies above 55 MeV agree to $\sim$0.1%, which is remarkable. Similar agreement is found for the energy leaked through the back of the shower calorimeter.

Response of the thin plastic veto detector to showers initiated by a photon originating in the target counter provides a stringent combined test of processes (c) and (d). This response clearly affects the overall detection efficiency for pion beta decays. ITS, GEANT and EGS4 results for this quantity are compared in Figure 11, bottom panel. The integrated yields above the MIP threshold differ by $\sim$0.5% of the total number of shower histories. However, raising the threshold by just 0.4 MeV improves the agreement to about 0.1% between ITS and GEANT and $\sim$0.3% between ITS and EGS4. We will study the mechanism of energy deposition in the narrow range just above the MIP threshold in order to understand and remove this discrepancy.

In order to isolate the effects (c), we simulated electromagnetic showers originating at the face of the CsI detector, by a perpendicularly incident 70MeV photon. We histogrammed the energy flow back across the CsI face in the direction opposite from that of the original photon momentum. The results are shown in Figure 12, top panel. We also histogrammed the response of the thin plastic veto counter to this back-splash, and plotted the results in the lower panel of Figure 12. The overall agreement found for both histogrammed quantities is quite satisfactory.

ITS and GEANT calculations of the total energy flow back across the CsI face agree extremely well, to better than 0.1% in integrated yield above 1 MeV. The EGS4 result is higher by almost 1% ; we intend to investigate the discrepancy. At any rate, the energy flow comparison is interesting only in terms of understanding the differences in the basic structure of the shower codes, but does not directly affect the calculation of detector efficiency.

A more relevant quantity from the standpoint of corrections to detection efficiency is the response of the PV counter. The results plotted in the lower panel of Figure 12 show that a very small fraction of the shower back-splash consists of charged particles, i.e., less than 1% of the histories register above the MIP threshold in the PV counter. Here, again, the agreement among the three codes is quite good. GEANT and EGS4 integrated yields above the MIP threshold are practically identical (they differ by fewer than 0.1% of the total number of histories). The ITS result, however, is slightly higher at large deposited energies. We have carefully selected the charged particle tracking parameters in GEANT to reproduce closely the Vavilov distribution in a thin counter. We are in the process of implementing the same procedure in ITS; we expect it to reduce the discrepancy found above.

One of the limitations of the results presented in this section and in Figures 11 and 12 is related to the calculational statistics. In order to achieve high accuracy, our simulations track all shower particles in very fine steps, and follow them until their energy becomes quite small, 10 keV. These choices make shower calculations very slow, particularly on VAX computers widely available until now. The slow speed limits our runs to about 10,000 shower histories per run. In order to remedy this situation, we have already transferred the GEANT code to a DECstation 5000 RISC computer. We plan to port ITS and EGS4 soon, as well. In the long term we intend to use only one code, GEANT, which includes the most comprehensive geometry package and interfaces with the CERN physics library routines. It is important, however, to benchmark it against the other two codes, particularly ITS, which was designed expressly to simulate low-energy showers, and has been shown in the past to describe experimental data slightly better than EGS4 [Ro-84]. If necessary, we shall improve GEANT's routines and algorithms for tracking of low-energy showers.

In summary, we have found that the processes affecting the detection efficiency of our system occur at the level of a few percent probability. The three available shower codes, GEANT, ITS and EGS4 agree in their calculations of detection efficiencies at the level of a few per mill, or better, depending on the process considered. We are pursuing these discrepancies further, and expect to narrow them down even more. Ultimately, however, these processes are subject to experimental measurement. We will evaluate our systematic uncertainties carefully during the setup and calibration part of the experiment, and will continue to monitor them during data taking.

2.10. Measurement of other decay processes

The experimental apparatus whose main features and specifications have been outlined above, is well suited for a range of other measurements besides the $\pi\beta$ decay. Of particular interest to us are the pion and muon radiative decays.

$\pi \rightarrow e\nu\gamma$ decay events with the positron and photon emitted almost back-to-back will be recorded alongside the $\pi\beta$ data. This is illustrated in Figure 10, which shows the sensitivity of our detector system to $\pi \rightarrow e\nu\gamma$ decays. The large-angle region of phase space is particularly sensitive to the "structure-dependent" part of the radiative decay, as well as to its interference with the inner bremsstrahlung part. It is likely that an extra trigger condition will be added to our main triggers to suit the study of $\pi \rightarrow e\nu\gamma$ decays. Given the high counting statistics of the planned $\pi\beta$ measurements, we should be able to improve the present parametrization of this decay process.

$\mu \rightarrow e\nu\overline{\nu}\gamma$ decays can, in principle, be studied equally well with our detector, with the advantage that they are more probable than $\pi \rightarrow e\nu\gamma$ decays. The muon radiative decay is particularly interesting because of its sensitivity to departures from $V - A$ theory. Its detection requires, however, tuning the beam for muons, reducing the stopping rate, accepting events during a later gate, and lowering the trigger thresholds. A certain sample of muon radiative decays will be present in our late-gate low-threshold prescaled triggers. We are currently studying the sensitivity of our detector to $\mu \rightarrow e\nu\overline{\nu}\gamma$ events.

Should we decide that opportunities to improve the present characterization of radiative and other rare pion and muon decay modes appear practical using the above described detector system, we will submit further proposals on those topics to the BV for consideration.

3. TIMETABLE AND RESOURCES

3.1. **Timetable**

The projected timetable for the experiment is:

In 1991/1992: obtain initial equipment funding; begin building a partial setup consisting of a subset of detectors (14 shower counters would be a minimum); work on developing the necessary beam characteristics; examine systematic aspects of the setup with in-beam measurements; in parallel, develop a tomography setup and evaluate crystals as they arrive; have the MWPC made.

In 1993: assemble a major portion of the setup and work up the π stop intensity gradually, working on the trigger and on understanding the systematics of all event types. Begin accumulating first data.

In 1994: begin running the "production" runs in the first phase.

In 1995: finish the first stage of data taking. Begin preparations for the second stage.

3.2. **An approximate budget**

All prices are in U.S. dollars. Listed are approximate prices for the major experimental items.

CsI crystals:	860 k$
phototubes and bases:	235 k$
electronics and HV:	208 k$
MWPC and its readout:	180 k$
separator refurbishing:	250 k$
Total:	1,750 k$

The available funds and equipment are as follows:

(a) The pure CsI detectors will be provided mostly by Tbilisi, and partly by UVa (about 15% of the modules). The UVa funds ($ 100 k) have already been committed; the detectors purchased have been used in the November 1989 test run, and since then recycled in order to be regrown for the new detector geometry. The portion of the Tbilisi cost which will have to be provided in hard currency is expected not to exceed $ 100 k. This represents a very substantial savings over the Western commercial prices.

(b) The Virginia group has already invested about $ 50 k into phototubes and bases for the calorimeter elements and active target readout. In addition, the US National Science Foundation is planning to fund the equipment necessary for this project at the level of about $ 400 k (pending peer review approval - the grant request is submitted simultaneously with this Update). These funds, along with the mentioned existing equipment, should cover the needs in electronics and photomultiplier tubes.

(c) The Dubna group will build the MWPC's and part of the readout electronics. The portion of electronics not provided by the Dubna group (primarily ADC's) will not exceed $ 100 k in cost.

(d) PSI will provide the required electrostatic crossed-field separator. In addition, PSI will spend up to $ 200 k on major equipment for this project (under (a) and (c) above). The rest of the cost will be borne by user-group sources.

4. REFERENCES

[Bar-85] R. Barbieri, C. Bouchiat, A. Georges, and P. Le Doussal, *Phys. Lett.* **156B** (1985) 348.

[Bar-86] R. Barbieri, C. Bouchiat, A. Georges, and P. Le Doussal, *Nucl. Phys.* **B269** (1986) 253.

[Bas-85] Proposal of the Basel-Cern-CEN Saclay-DAP Athens-Democritos-ETH-Fribourg-Liverpool-SIN-Stockholm-Tessaloniki Collaboration, CERN/PSCC/85-6, PSCC/P 82

[Bop-86] P. Bopp, B. Dubbers, L. Hornig, J. Last, H. Schütze, S.J. Freedman, and O. Schärpf, *Phys. Rev. Lett.* **56** (1986) 919.

[Bor-82] K. Borer, G. Czapek, A. Flückinger, D. Frei, B. Hahn, E. Hugentobler, R. Moning, U. Moser, E. Ramseyer, H. Scheidiger, R. Abela and E. Steiner, SIN Proposal R-82-04.1, August 1982, *unpublished.*

[Bor-83] K. Borer *et al.* , SIN Proposal R-82-04.4, April 1983, *unpublished.*

[Coc-61] V.T. Cocconi, T. Fazzini, G. Fidecaro, M. Legros, N.H. Lipman and A.W. Merrison, *Nuovo Cim.* **22** (1961) 494.

[Cra-86] J.F. Crawford, M. Daum, R. Frosch, B. Jost, P.R. Kettle, R.M. Marshall and K.O.H. Ziock, *Phys. Rev. Lett.* **56** (1986) 1043.

[Cra-88] J.F. Crawford, M. Daum, R. Frosch, B. Jost, P.R. Kettle, R.M. Marshall, B.K. Wright and K.O.H. Ziock, *Phys. Lett.* **213B** (1988) 391.

[Dau-87] M. Daum, P.R. Kettle, B. Jost, R.M. Marshall, R.C. Minehart, W.A. Stephens, and K.O.H. Ziock, *Phys. Rev.* **D36** (1987) 2624.

[Dep-68] P. Depommier, J. Duclos, J. Heintze, K. Kleinknecht, H. Riesenberg and V. Soergel, *Nucl. Phys.* **B4** (1968) 189.

[Don-87] J.F. Donoghue, B.R. Holstein and S.W. Klimt, *Phys. Rev. D* **35** (1987) 934.

[Dru-87] E.G. Drukarev and M.I. Strikman, *Phys. Lett.* **186B** (1987) 1.

[Ero-90] Erozolimskiĭ, A. Kuznetsov, I.A. Kuĭda, Yu. A. Mostovoĭ and I.V. Stepanenko, *Yad. Fiz.* **52**, 1583 (1990).

[Fey-58] R.P. Feynman and M. Gell-Mann, *Phys. Rev.* **109** (1958) 193

[Har-90] J.C. Hardy, I.S. Towner, V.T. Koslowsky, E. Hagberg and H. Schmeing, *Nucl. Phys.* **A509**, 429 (1990).

[Hig-83] V. Highland, in *"Physics with LAMPF II"*, Los Alamos National Laboratory Report No. LA-9798-P, 1983, p. 302.

[Jau-87] W. Jaus and G. Rasche, *Phys. Rev. D* **35** (1986) 3420.

[Käl-64] G. Källén, *Elementary Particle Physics*, (Addison- Wesley, Reading, Mass. 1964) pp. 400 ff.

[Ket-90] P.R. Kettle, *private communication*, 1990

[Kub-88] S. Kubota, S. Sakuragi, S. Hashimoto, J. Ruan, *Nucl. Inst. and Meth.* **A268** (1988) 275.

[Las-88] J. Last, M. Arnold, J. Döhner, B. Dubbers, and S.J. Freedman, *Phys. Rev. Lett.* **60** (1988) 995.

[Mar-86] W.J. Marciano and A. Sirlin, *Phys. Rev. Lett.* **56** (1986) 22.

[Mar-87] W.J. Marciano and A. Sirlin, *Phys. Rev. D* **35** (1987) 1672.

[McF-85] W.K. McFarlane, L.B. Auerbach, F.C. Gaille, V.L. Highland, E. Jastrzembski, R.J. Macek, F.H. Cverna, C.M. Hoffman, G.E. Hogan, R.E. Morgado and R.D. Werbeck, *Phys. Rev. D* **32** (1985) 547.

[Nel-85] W.R. Nelson, H. Hirayama and D.W.O. Rogers, SLAC-Report-265, December 1985.

[Num-88] T. Numao, *private communication.*

[Ore-82] M. Oreglia, E. Bloom, F. Bulos, R. Chestnut, J. Gaiser, G.Godfrey, C.Kiesling, W. Lockman, D.L. Scharre, R. Partridge, C. Peck, F.C. Porter, D. Antreasyan, Yi-Fan Gu, W. Kollmann, M. Richardson, K. Strauch, K. Wacker, D. Aschman, T. Burnett, C. Newman, M. Cavalli- Sforza, D. Coyne, D. Sadrozinski, R. Hofstadter, I. Kirkbride, H. Kolanoski, K. Königsmann, A. Liberman, J. O'Reily, B. Pollock and J. Tompkins, *Phys. Rev. D* **25** (1982) 2259.

[Orm-85 W.E. Ormand and B.A. Brown, *Nucl. Phys.* **A440** (1985) 274.

[Orm-89] For the most up-to-date discussion of δ_C see: W.E. Ormand and B.A. Brown, *Phys. Rev. Lett.* **62** (1989) 866.

[Ro-84] D.W.O. Rogers, *Nucl. Inst. Meth.* **227** (1984) 535.

[Sir-78] A. Sirlin, *Rev. Mod. Phys.* **50** (1978) 573.

[Sir-86] A. Sirlin and R. Zucchini, *Phys. Rev. Lett.* **57** (1986) 1994.

[Sir-87a] A recent review of the status of radiative corrections to Fermi decays, including references to previous work, is found in: A. Sirlin, *Phys. Rev. D* **35** (1987) 3423.

[Sir-87b] A. Sirlin, *Comments Nucl. Part. Phys.* **17**, 279 (1987).

[Sir-89] A. Sirlin, *private communication*, 1989.

[Tho-88] E.D. Thorndike and R.A. Poling, *Phys. Rep.* **157** (1988) 183.

[Tow-77] I.S. Towner, J.C. Hardy and M. Harvey, *Nucl. Phys.* **A284** (1977) 269.

[Wil-78] D.H. Wilkinson, in *"Nuclear Physics with Heavy Ions and Mesons"*, ed. by R. Balian, M. Rho and G. Ripka (North Holland, Amsterdam, 1978), p. 877.

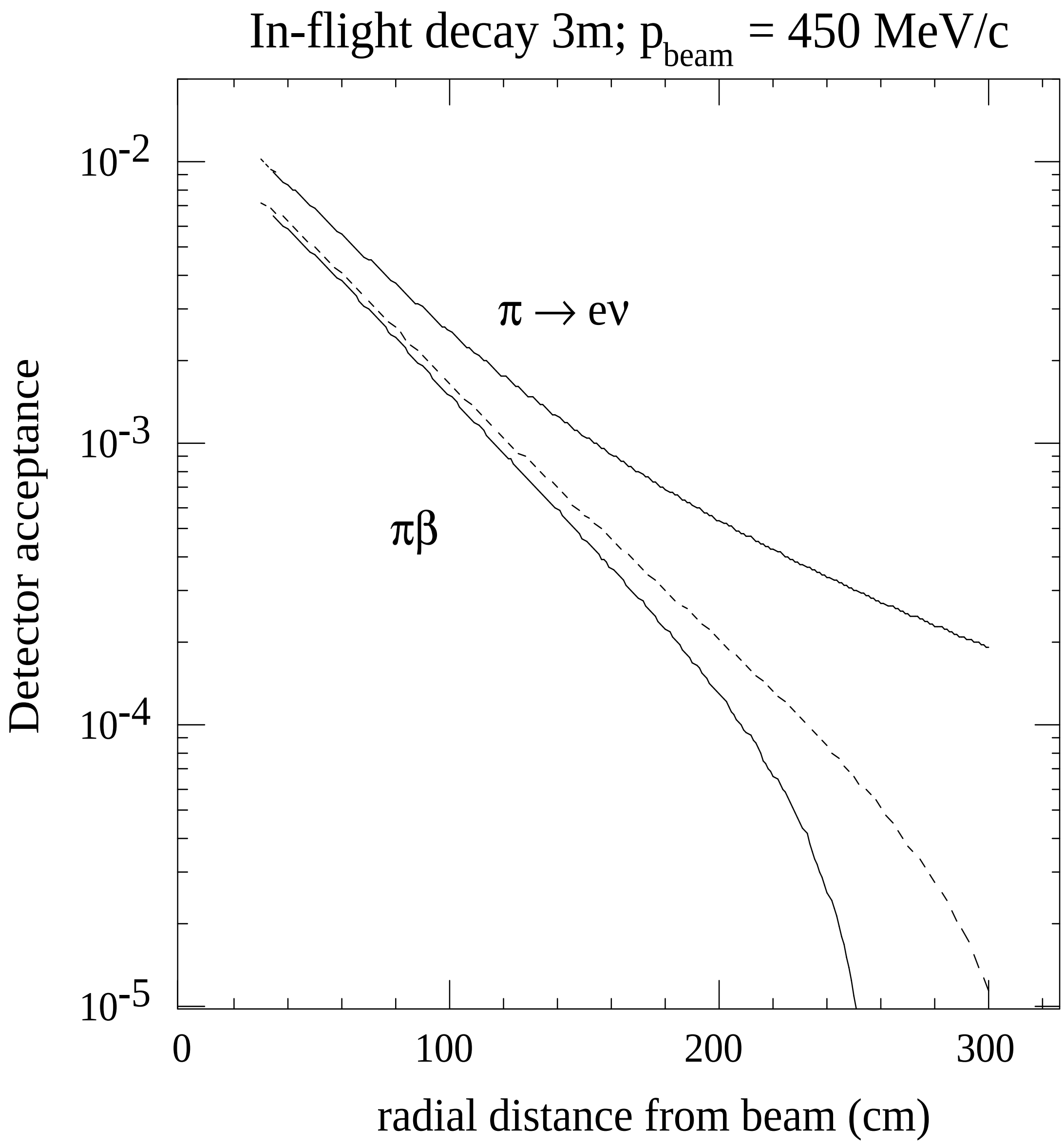

Figure 1. Calculation of acceptance for an in-flight decay apparatus (a "wall" detector) assuming a 3 m decay path and beam momentum of 450 MeV/c. Shown are acceptances for both $\pi\beta$ and $\pi \to e\nu$ decays. The dashed line shows the change in $\pi\beta$ acceptance corresponding to extending the detector inward radially by 5 cm at the center.

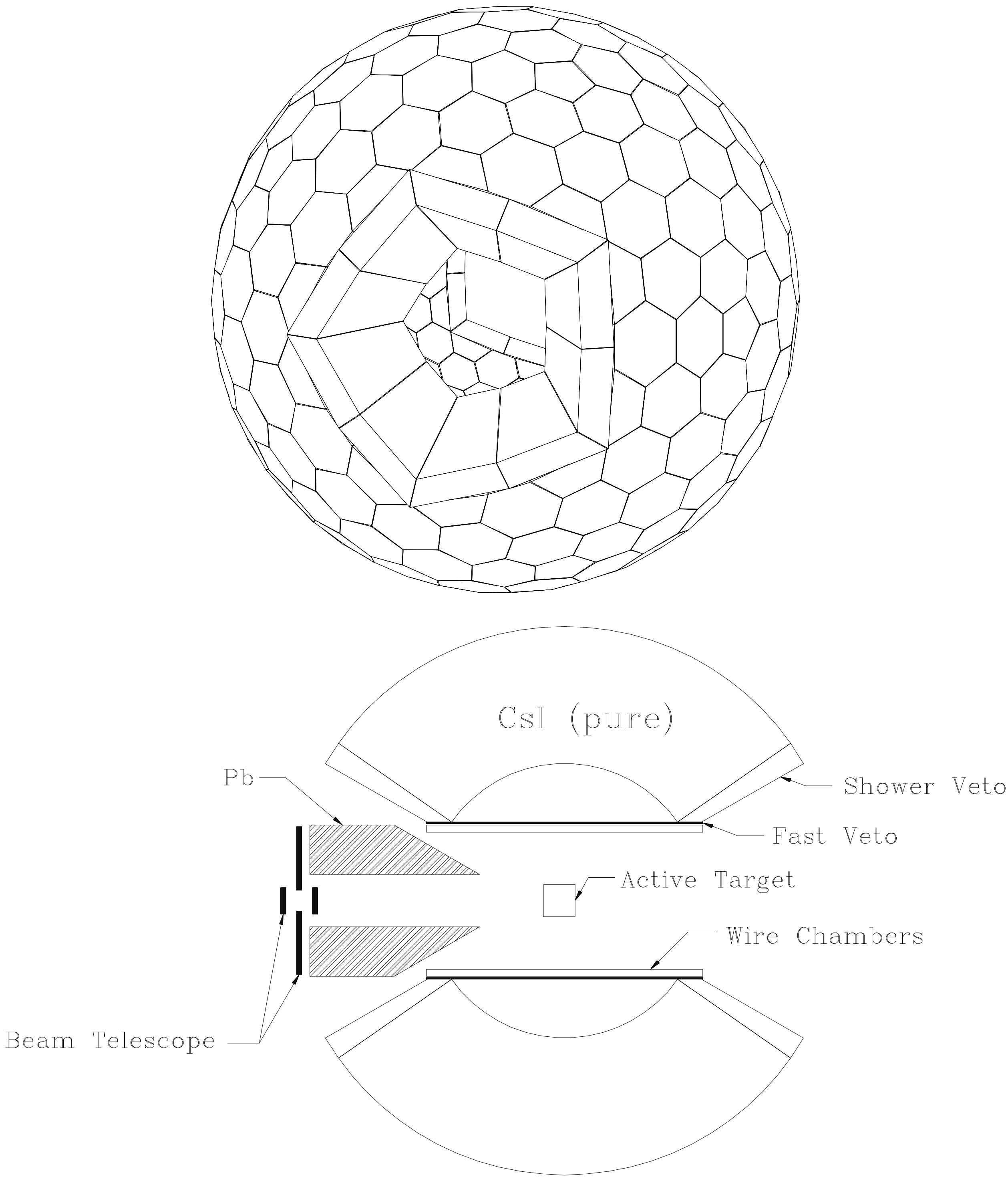

Figure 2. A simplified sketch of the experimental setup showing a view of the shower calorimeter and its cross section designating the main components.

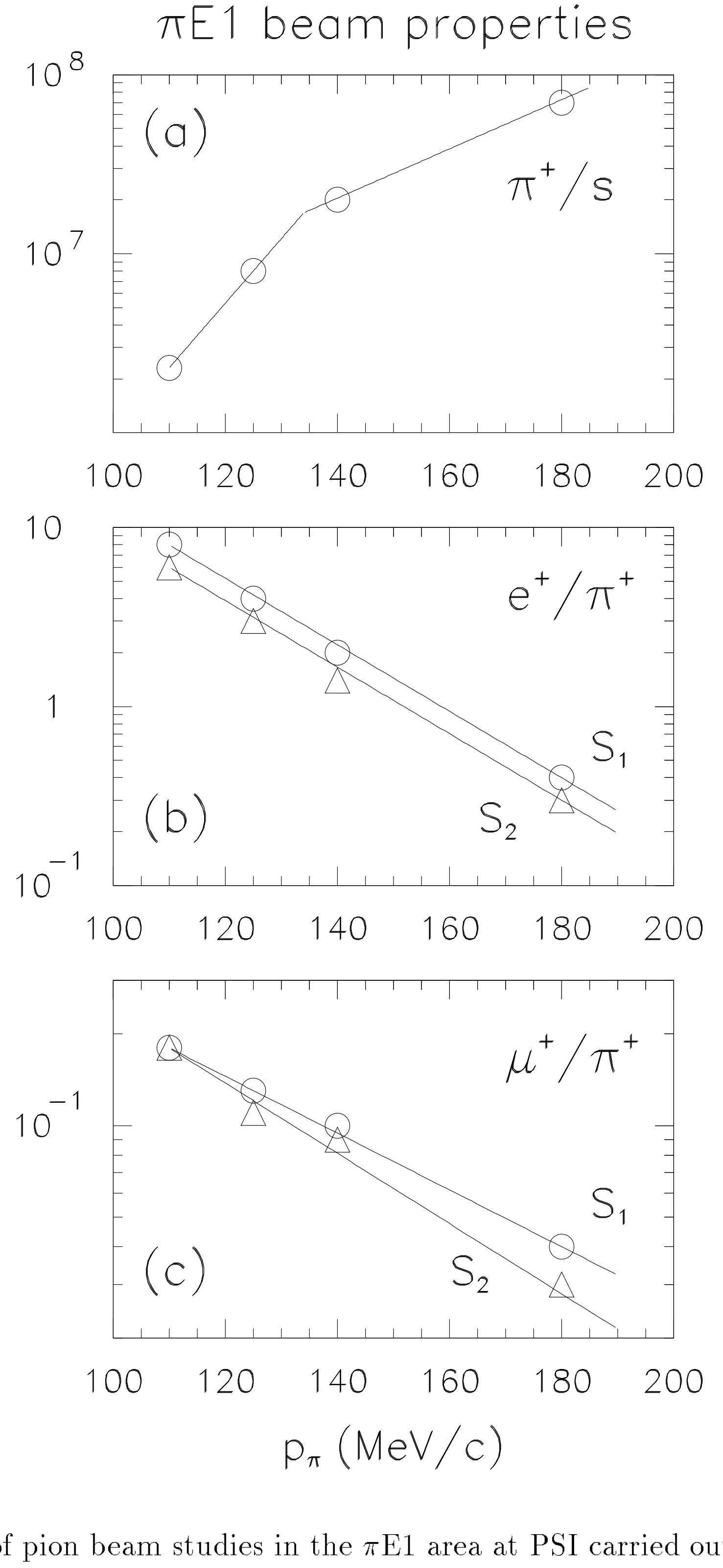

Figure 3. Results of pion beam studies in the πE1 area at PSI carried out in 1989: (a) pion current per 100 μA of primary beam registered on a 40 mm $\times$ 40 mm detector; (b), and (c), e^+/π^+ and μ^+/π^+ contaminations, respectively, measured on a small detector (S1, $\phi = 1$ mm, and S2, 40 mm $\times$ 40 mm). Curves are drawn only to guide the eye.

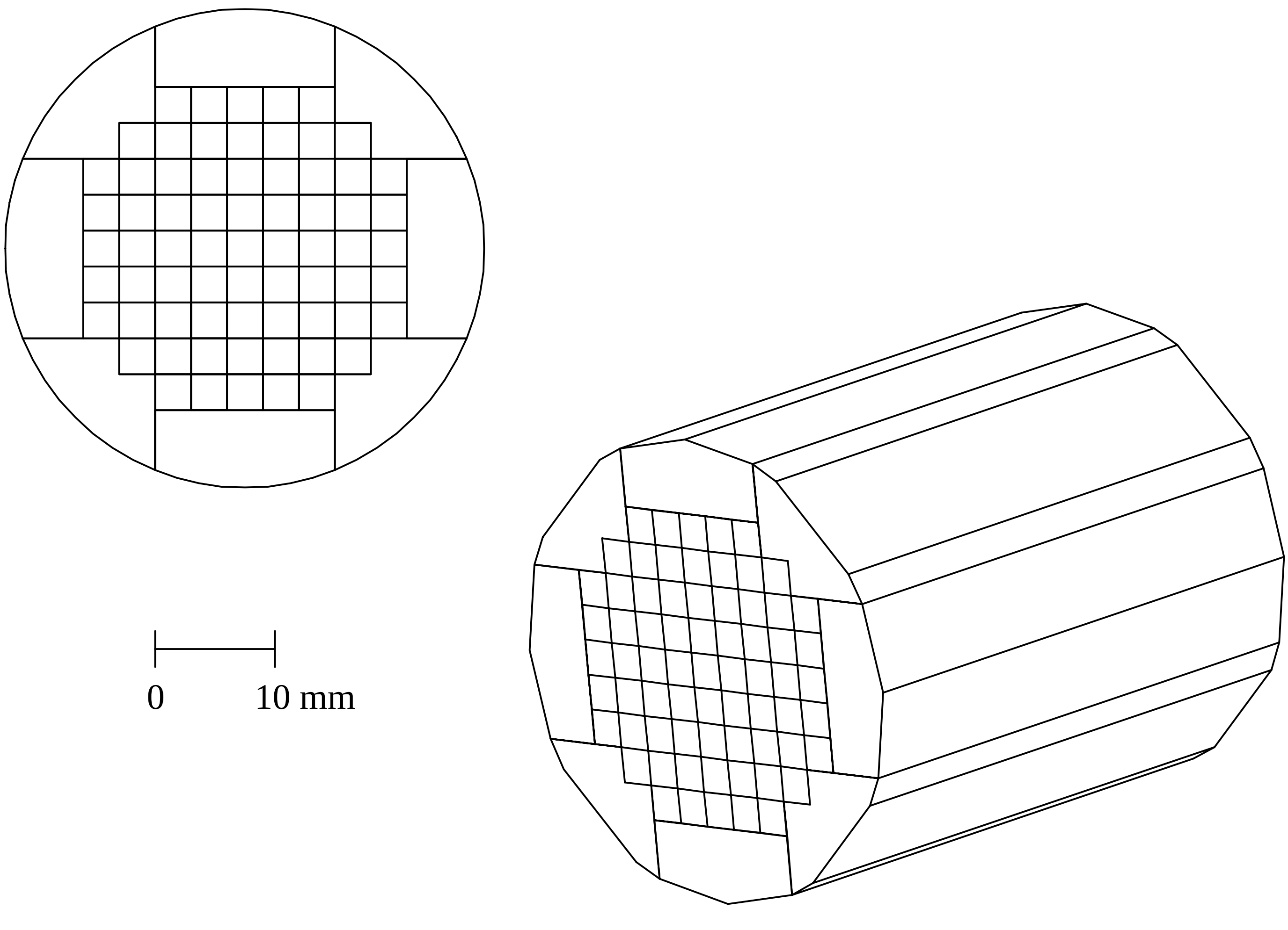

Figure 4. Design drawing of the active target.

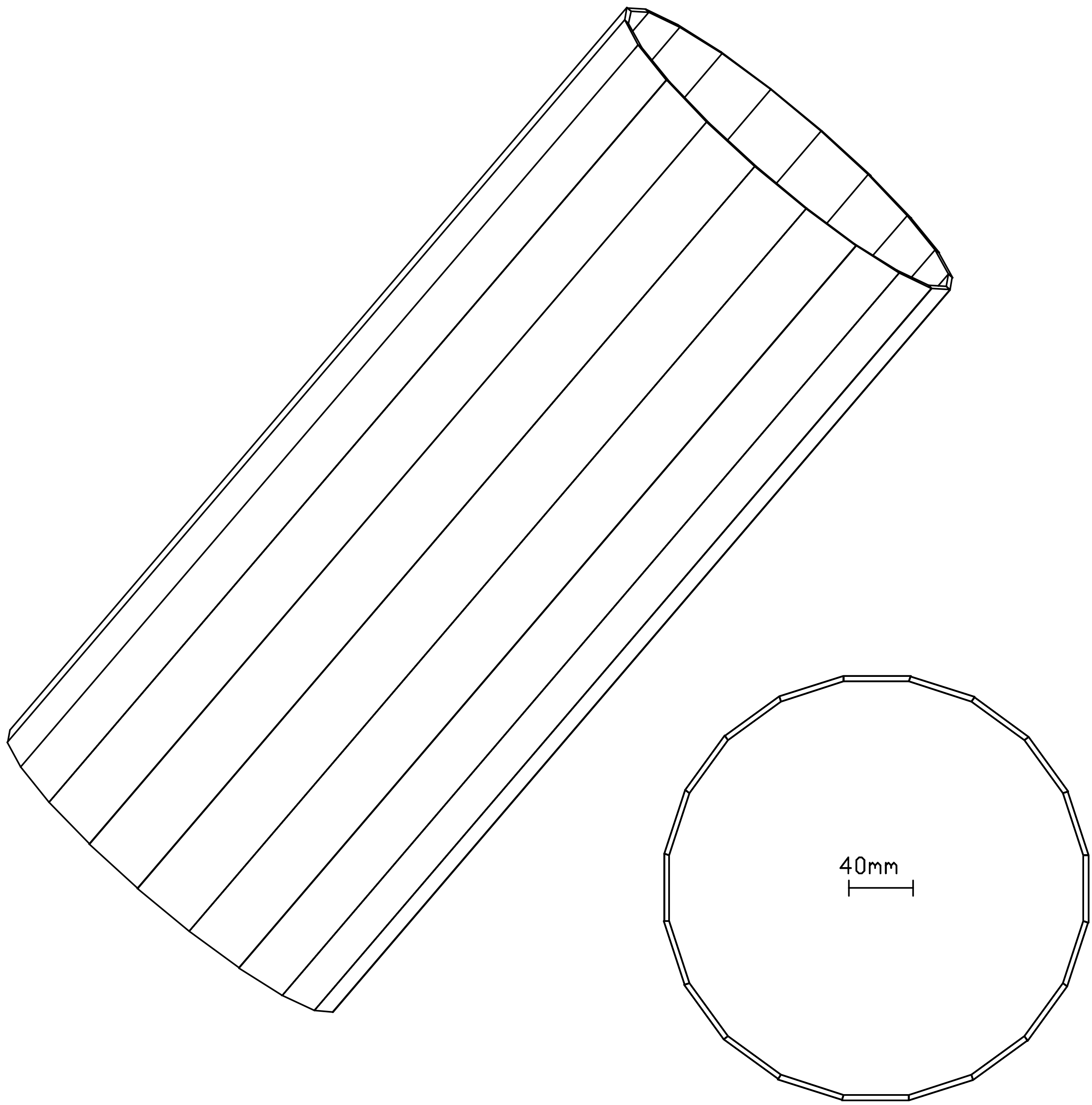

Figure 5. A drawing of the fast plastic veto counter.

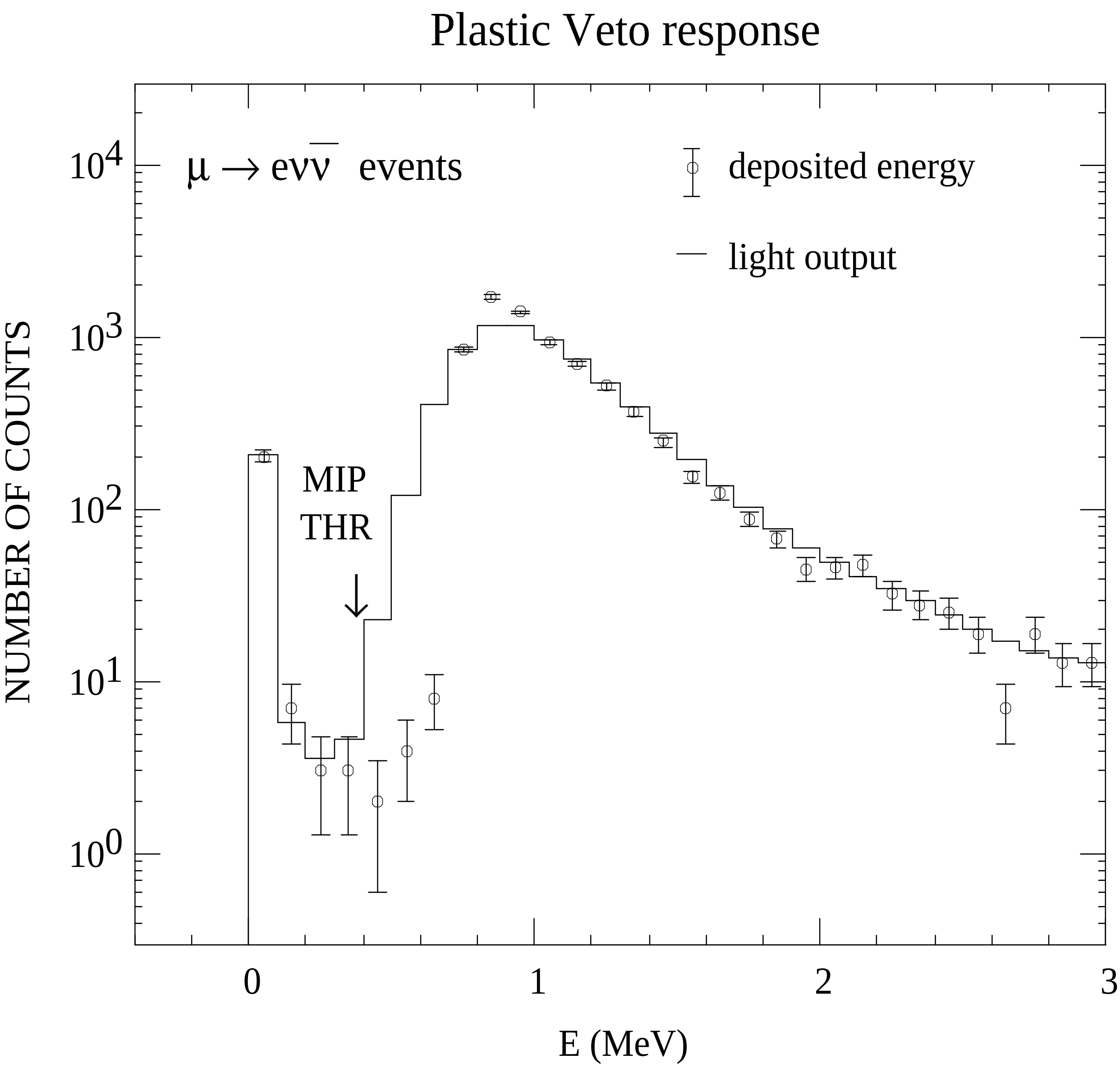

Figure 6. Energy deposition (data points) and light output (histogram) for Michel events in the fast plastic veto (PV) counter. The arrow denotes a suitable choice for the MIP threshold.

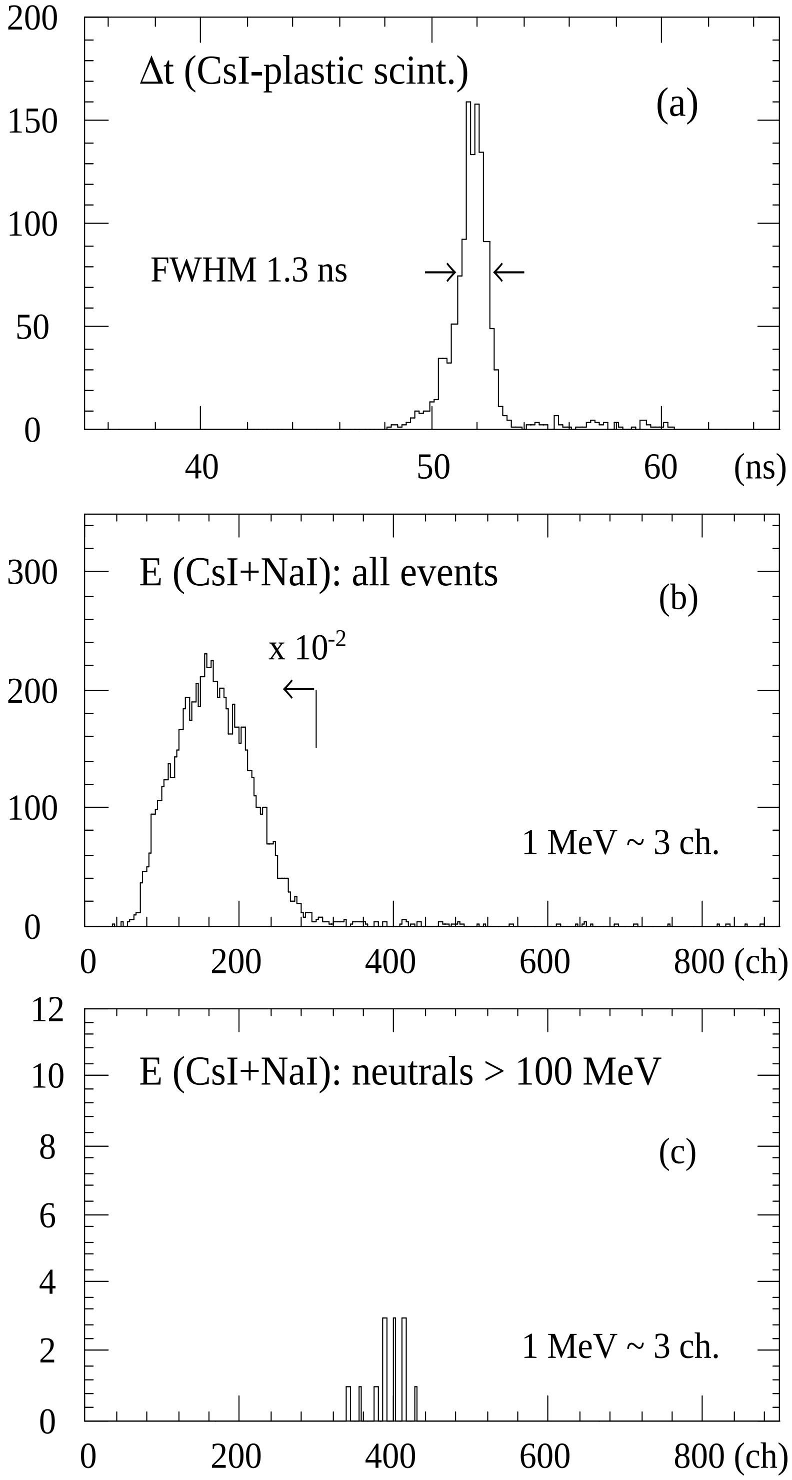

Figure 7. Spectra obtained during the development run in November 1989: (a) timing of a CsI module relative to a plastic scintillator counter (scale: 20 ch/ns), (b) sum energy spectrum of the NaI and CsI arms, including charged particle events, and (c) same as (b) for neutral showers only, exceeding a ~100 MeV threshold. The energy scale in (b) and (c) is approximately 3 channels/MeV. For details and discussion see Section 2.7.

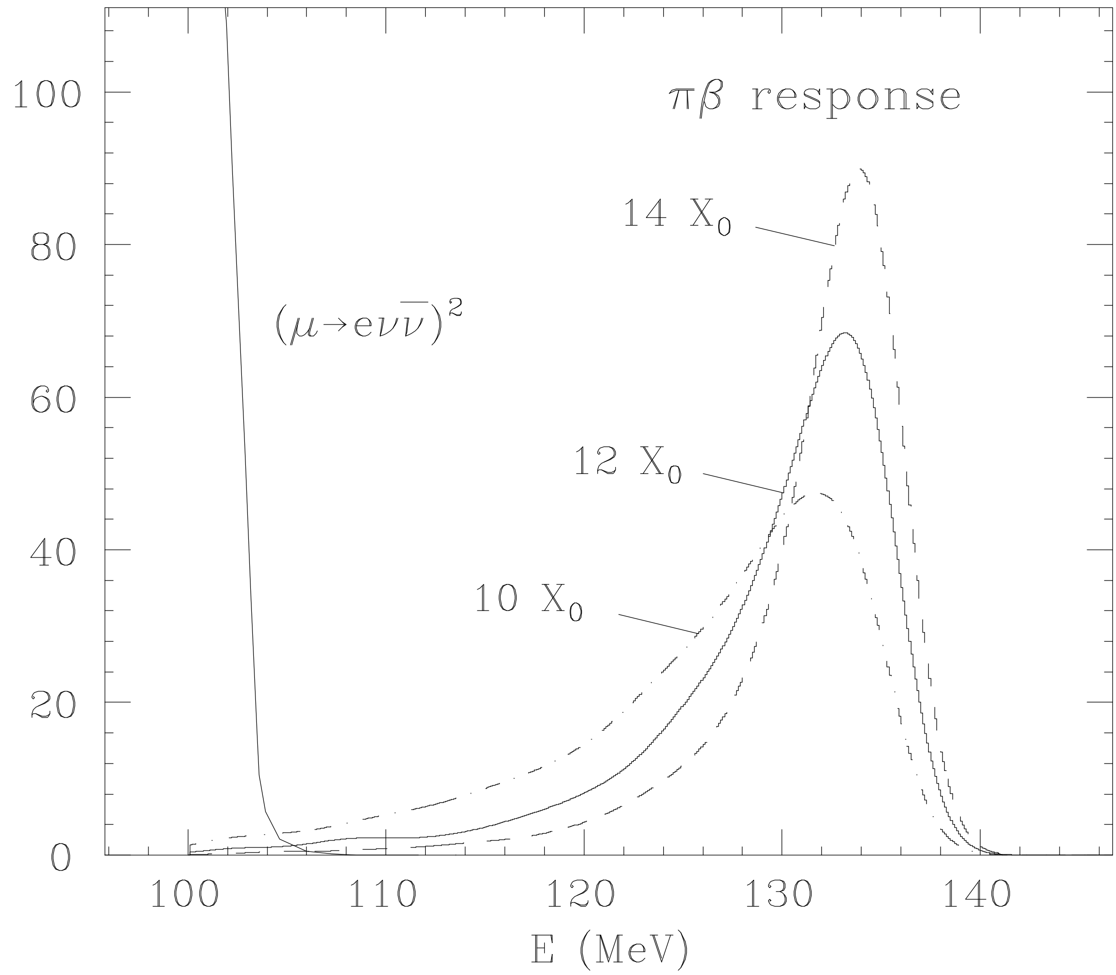

Figure 8. GEANT calculation of the CsI shower calorimeter response to $\pi\beta$ decay events satisfying all appropriate cuts, for three detector thicknesses: 10, 12 and 14 radiation lengths, respectively. Also included is the CsI response to accidentally coincident Michel decays in the target. Curves shown include smearing due to light collection statistics and nonuniformity.

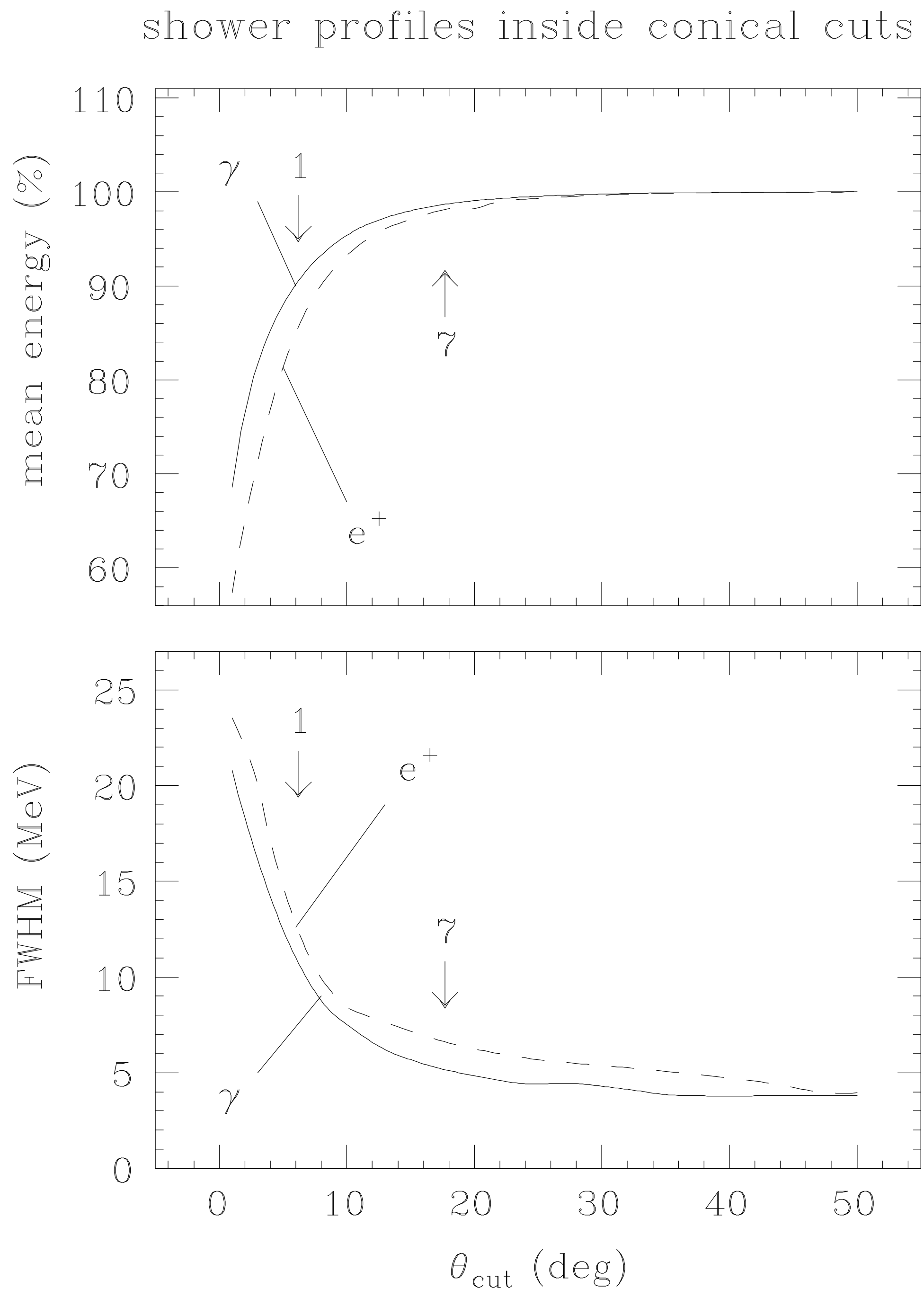

Figure 9. Profiles of electromagnetic shower spreading in the CsI calorimeter. The CsI geometry is shown schematically in Figure 2. Histogrammed are first and second moments (mean energies and FWHM's) of the spectra of energy deposited by the shower inside a conical fiducial subvolume of the calorimeter. The conical subvolumes are defined by their half-opening angles, θ_{cut}. Showers were initiated by 70 MeV photons (solid curves) and positrons (dashed curves). Calculations were performed using the computer code GEANT.

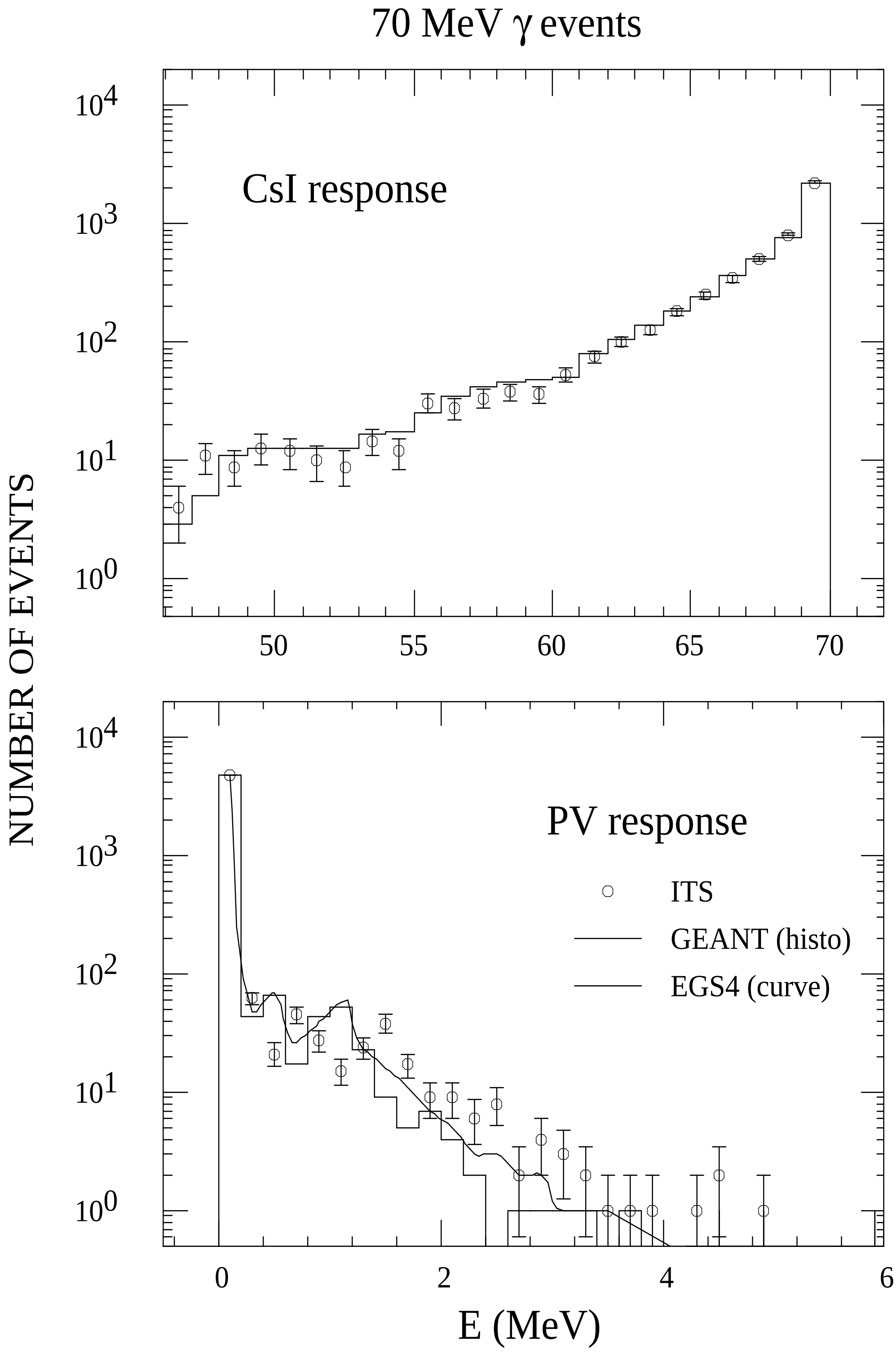

Figure 10. Comparison of ITS, GEANT and EGS4 simulations of energy deposition distributions in CsI and fast plastic veto (PV) counters, in a simplified planar geometry. Showers were initiated by 70 MeV photons. See Section 2.9. for details and discussion.

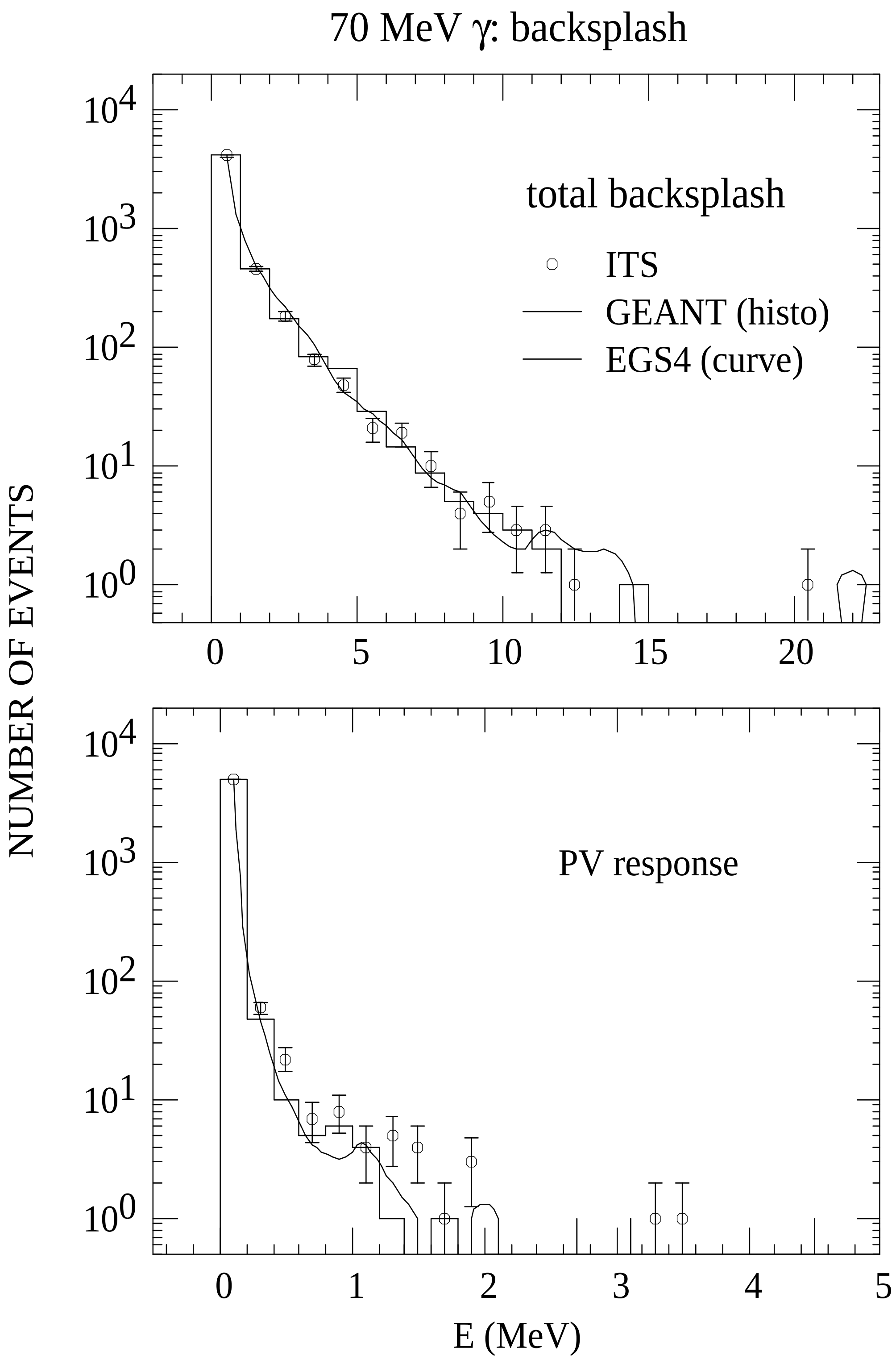

Figure 11. Comparison of ITS, GEANT and EGS4 simulations of energy flow reflected back from the CsI detector (top). A fraction of the articles flowing back register in the fast plastic veto (PV) counter. The distribution of energies deposited in PV is shown in the bottom panel. Showers were initiated by 70 MeV photons. See Section 2.9. for details and discussion.

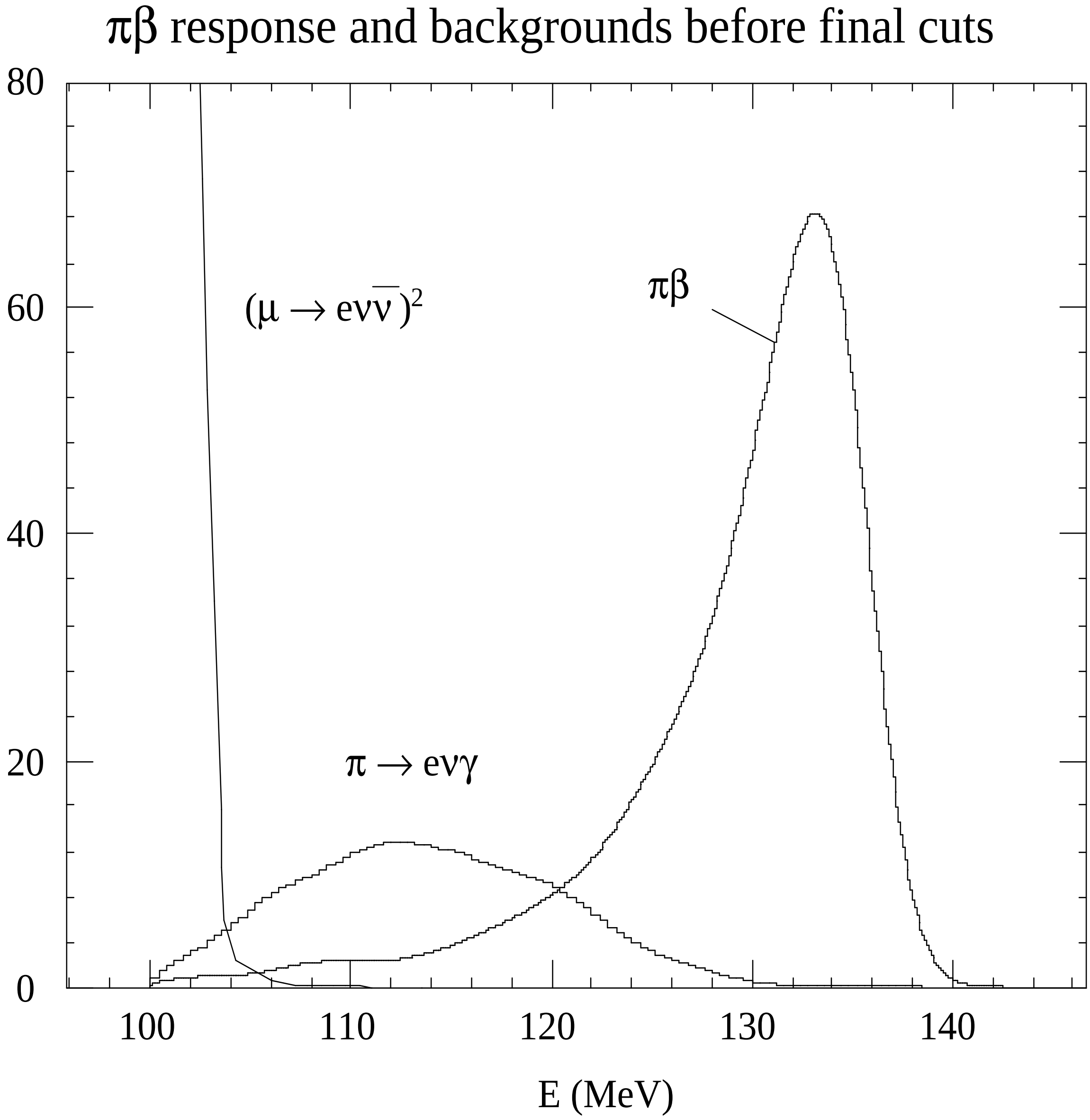

Figure 12. Results of simulations of $\pi\beta$ trigger events at the pion stopping rate of $5 \times 10^6 \pi/s$. Line-Shapes shown include the effects of photoelectron statistics and optical nonuniformities in the crystals. The trigger threshold would be at around 110 MeV and would largely exclude the $\mu \to e\nu\overline{\nu}$ events.